Parameterization and Surface Data Improvements and New Capabilities for the Community Land Model Urban (CLMU)

K. W. Oleson & J. Feddema

October 2019

JAMES | Journal of Advances in Modeling Earth Systems

RESEARCH ARTICLE
10.1029/2018MS001586

Special Section:
Community Earth System Model version 2 (CESM2) Special Collection

Parameterization and Surface Data Improvements and New Capabilities for the Community Land Model Urban (CLMU)

K. W. Oleson[1] and J. Feddema[2]

[1]National Center for Atmospheric Research, Boulder, Colorado, [2]University of Victoria, Victoria, BC, Canada

Abstract The Community Land Model Urban (CLMU) is an urban parameterization developed to simulate urban climate within a global Earth System Model framework. This paper describes and evaluates parameterization and surface data improvements, and new capabilities that have been implemented since the initial release of CLMU in 2010 as part of version 4 of the Community Land Model (CLM4) and the Community Earth System Model (CESM®). These include: 1) an expansion of model capability to simulate multiple urban density classes within each model grid cell; 2) a more sophisticated and realistic building space heating and air conditioning submodel; 3) a revised global dataset of urban morphological, radiative, and thermal properties utilized by the model, including a tool that allows for generating future urban development scenarios, and 4) the inclusion of a module to simulate various heat stress indices. The model and data are evaluated using observed data from five urban flux tower sites and a global anthropogenic heat flux (AHF) dataset. Generally, the new version of the model simulates urban radiative and turbulent fluxes, surface temperatures, and AHF as well or better than the previous version. Significant improvements in the global and regional simulation of AHF are also demonstrated that are primarily due to the new building energy model. The new model is available as part of the public release of CLM5 and CESM2.0.

Plain Language Summary The Community Land Model Urban (CLMU) is a modeling system designed to simulate the local climate of urban areas around the world. The model has proven to be a useful tool in prior studies that highlight projected changes in urban climate, human thermal comfort, and building energy due to future global climate change. Here we describe changes to the model and new model capabilities designed to enhance model efficacy. These include: 1) the ability to simulate the local climate of different urban classes (e.g., high rise building areas and apartment complexes); 2) an improved space heating and air conditioning submodel to determine building energy demand; 3) a revised dataset of urban properties (e.g., building height, roof color) utilized by the model, including a tool that allows for the testing of future urban development scenarios, and 4) the inclusion of a module to simulate various heat stress indices that relate to human thermal comfort. Generally, the new version of the model simulates urban climate and building energy as well or better than the previous version. The improved model should prove useful for investigating the combined effects of future global climate change and urbanization on people that live in urban areas.

Key Points:
- Parameterization and surface data improvements, and new capabilities for the Community Land Model Urban are described and evaluated
- Simulation of urban radiative and turbulent fluxes, surface temperatures, and anthropogenic heat flux is generally improved
- The new capabilities allow for more efficient simulation of different urban density classes and exploring future urban development scenarios

Supporting Information:
- Supporting Information S1

Correspondence to:
K. W. Oleson,
oleson@ucar.edu

Citation:
Oleson, K. W., & Feddema, J. (2020). Parameterization and surface data improvements and new capabilities for the Community Land Model Urban (CLMU). *Journal of Advances in Modeling Earth Systems*, *12*, e2018MS001586. https://doi.org/10.1029/2018MS001586

Received 6 DEC 2018
Accepted 20 JUN 2019
Accepted article online 19 OCT 2019

Author Contributions:
Conceptualization: K. W. Oleson, J. Feddema
Data curation: K. W. Oleson, J. Feddema
Formal analysis: K. W. Oleson
Funding acquisition: K. W. Oleson
Investigation: K. W. Oleson
(continued)

1. Introduction

The numerical simulation of urban climate has received a great deal of attention in the last several years as evidenced by the 32 urban models that were participants in a recent intercomparison exercise (Grimmond et al., 2011). One model participating in this exercise, the Community Land Model Urban (CLMU), has a unique purpose in simulating local urban climate as an operational component of a global climate model. CLMU is the urban submodel within the Community Land Model (CLM) and CLM is the land component used in the Community Earth System Model version 2 (CESM2) (http://www.cesm.ucar.edu/models/cesm2/). The publically available and supported CLMU (http://www.cesm.ucar.edu/models/cesm2.0/land/), in combination with the CLM and the CESM, allows for the capability of simulating the local urban environment for present-day climate and climate change scenarios such as those described by the Coupled Model Intercomparison Project phase 5 (CMIP5) (Oleson, 2012). In particular, the model simulates energy and water balances as well as air temperature and humidity in urban areas where the majority of the

Methodology: K. W. Oleson, J. Feddema
Project administration: K. W. Oleson
Resources: K. W. Oleson
Software: K. W. Oleson, J. Feddema
Supervision: K. W. Oleson, J. Feddema
Validation: K. W. Oleson
Visualization: K. W. Oleson
Writing - original draft: K. W. Oleson
Writing – review & editing: K. W. Oleson, J. Feddema

world's population lives and works. The purpose of the model is not to simulate specific cities but rather to use highly idealized representations of urban canyons to investigate how local urban climates vary in different climatic conditions across the world and to better evaluate potential interactions between local urban climates and in relation to regional and global scale climate change.

The purpose of this paper is to describe the recent parameterization and surface data improvements, and new capabilities that have been implemented since the initial release of CLMU within version 4 of the Community Land Model (CLM4) (Lawrence et al., 2011; Oleson, Lawrence, et al., 2010). These include: 1) an expansion of model capability to simulate multiple urban density classes within each model grid cell instead of the previously used spatially dominant urban density class in a gridcell; 2) a more sophisticated and realistic building space heating and air conditioning submodel that prognoses interior building air temperature; 3) a revised global dataset of urban morphological, radiative, and thermal properties utilized by the model, including improvements that allow for generating more detailed future urban development scenarios; and 4) a module of heat stress indices calculated online in the model to assess human thermal comfort. The new urban model has been developed within the framework of the most recent released version of CLM (CLM5; Lawrence et al., 2019). We refer to this new version of the urban model herein as CLMU5.

Section 2 first provides a brief overview of the version of CLMU in CLM4. The new improvements and capabilities listed above are described in detail in sections 3, 4, 5, and 6, respectively. In section 7 we describe simulations that were designed to evaluate and test these improvements and demonstrate new capabilities, results are presented in section 8.

2. Overview of CLMU in CLM4

CLMU was initially described in Oleson, Bonan, Feddema, Vertenstein, & Grimmond (2008), Oleson, Bonan, Feddema, & Verte (2008). This is the same version of CLMU that is implemented in CLM4 as documented in Oleson, Bonan, et al. (2010) (hereinafter CLMU4). A brief description is provided here for context in the discussions in subsequent sections.

Grid cells in CLM4 can be composed of up to five landunits; vegetated, glacier, wetland, lake, and urban, where CLMU4 serves as the parameterization for the urban landunit. The urban landunit has five components; roof, sunlit wall, shaded wall, and pervious (e.g., to represent residential lawns and parks within the urban boundaries) and impervious (e.g., to represent roads, parking lots, sidewalks) surfaces on the canyon floor. The urban components are arranged in an urban canyon configuration in which the canyon geometry is described by building height and street width (see Fig. 2 in Oleson, 2012).

Trapping of radiation in the urban canyon is accounted for by parameterizations of reflection and absorption of solar radiation, and the absorption and emission of longwave radiation. Separate energy balances, including turbulent fluxes, and surface temperatures are determined for each of the five canyon surfaces. A one-dimensional heat conduction equation is solved numerically for a multi-layer column to determine conduction fluxes into and out of each surface. The lower (internal) boundary conditions for roofs and walls are determined by an approximation of internal building temperature held between prescribed maximum and minimum temperatures. The amount of energy required to be added to bring the interior building temperature up to the minimum temperature and the amount of energy required to be removed from the building interior to reduce the interior building temperature to the maximum temperature are designated as the space heating and air conditioning fluxes, respectively. The heat removed by air conditioning is added as wasteheat (sensible heat) to the canyon floor. Wasteheat from inefficiencies in the heating and air conditioning equipment and from energy lost in the conversion of primary energy sources to end use energy is also added as sensible heat to the canyon floor. Turbulent (sensible and latent heat) and storage heat fluxes and surface and internal structure temperatures (e.g., 15 layers for roofs and walls) are calculated for each urban surface. Momentum fluxes are determined for the entire urban surface using a roughness length and displacement height appropriate for the urban canyon morphology characteristics and stability formulations from CLM.

Roof and canyon floor hydrology are simulated while walls are hydrologically inactive. A snowpack can form on the active surfaces. Liquid water is allowed to pond on roofs and canyon floors which supports evaporation. Snowmelt water or water in excess of the maximum ponding depth runs off and is eventually transported to the ocean using the River Transport Model (RTM) in CLM. The hydrology for pervious canyon

floor is parameterized similarly to CLM4 soil. However, the vegetation-related processes associated with evaporation of canopy intercepted water and transpiration are not explicitly represented. Instead, evaporation is parameterized by a bulk scheme in which evaporation is a function of the wetness of the entire soil column and water is removed from each soil layer (Oleson, Bonan, et al., 2010).

The heat and moisture fluxes from each surface interact with each other through a bulk air mass that represents air in the urban canopy layer for which temperature, humidity, and wind speed are estimated. The air temperature can be compared with that from surrounding vegetated (rural) surfaces in the model to ascertain heat island characteristics. The CLMU is forced either with output from a host atmospheric model [e.g., the Community Atmosphere Model (CAM) or observed forcing (e.g., reanalysis or field observations)]. The atmospheric forcing required is air temperature and humidity, wind speed, precipitation, and downward solar and longwave radiation from the lowest level of the atmosphere model. The model produces sensible heat, latent heat, momentum fluxes, and emitted longwave and reflected solar radiation that are area averaged with fluxes from nonurban landunits to provide gridcell-averaged fluxes to the atmosphere.

Present-day urban extent and urban properties are provided by the global dataset developed by Jackson et al. (2010) (hereinafter J2010). Spatial extent of urban areas is derived from a population density dataset at 1km spatial resolution. Four general levels of urbanization are defined [referred to here as urban density classes; tall building district (TBD), and high, medium, and low density (HD, MD, LD)]. Each 1km pixel is classified as one of the four density classes. A dataset of building morphological (e.g., building height to street width ratio, roof fraction, average building height, and pervious fraction of canyon floor), thermal (e.g., thermal conductivity and heat capacity of materials making up roofs, walls, and roads), and radiative (e.g., albedo and emissivity) characteristics, as well as building interior maximum and minimum thermostat settings that control the need for heating and air conditioning was compiled (see blue boxplots of urban properties in Figure 1). These properties can be defined uniquely for thirty-three regions of similar physical and social characteristics spanning the global land surface and for each density class. All 1km pixels of a given density class falling within a given region are assigned the same properties. In CLMU4, the model is limited to simulating a single urban landunit per gridcell, chosen to be the dominant density class by area; and the LD class is not used because these areas tend to be suburban and not suitable for simulation in an urban canyon model. This means that urban areas globally are almost exclusively of the medium density class.

3. Multiple urban density classes

As noted above, the CLMU4 is not able to take full advantage of the capability of the J2010 dataset to represent multiple urban density classes within a gridcell. In the updated CLMU5, the single urban landunit is expanded to three urban landunits representing the TBD, HD, and MD classes. The TBD class as described in J2010 is defined as an area of at least 1 km^2 with buildings greater than or equal to ten stories tall, with a small pervious fraction (i.e., 5-15% of plan area). The HD class can encompass commercial, residential, or industrial areas that are characterized by buildings three to ten stories tall with a pervious fraction typically in the range of 5-25%. The MD class is usually characterized by row houses or apartment complexes one to three stories tall with a pervious fraction of 20-60%. The LD class is still not modelled pending development of a model more suitable for the vegetation-dominated nature of the LD class rather than the urban canyon model used here. As in previous versions of the model, the three landunits operate independently within the grid cell (as do other landunits such as vegetated, glaciers, lakes, and wetlands) and their fluxes are area-averaged to yield gridcell fluxes to the atmosphere.

Urban extent for the TBD, HD, and MD classes is available from the J2010 dataset as binary data (urban or no-urban) globally at a spatial resolution of 0.00833° (~1 km at the equator). However, the finest resolution accepted by the CLM tool that creates surface datasets at the required spatial resolutions for use by CLM (*mksurfdata_map*) is 0.05° latitude by 0.05° longitude (~30 km^2 at the equator). Thus, the 1 km extent data is aggregated to generate percent cover of the TBD, HD, MD urban density classes at a resolution of 0.05°. The percent cover data is then combined with the J2010 urban properties data that varies by geographic region (thirty-three in number) and density class (three) by a newly developed tool set (Toolbox for Human-Earth System Integration & Scaling [THESIS]; see section 5) to yield a complete urban surface

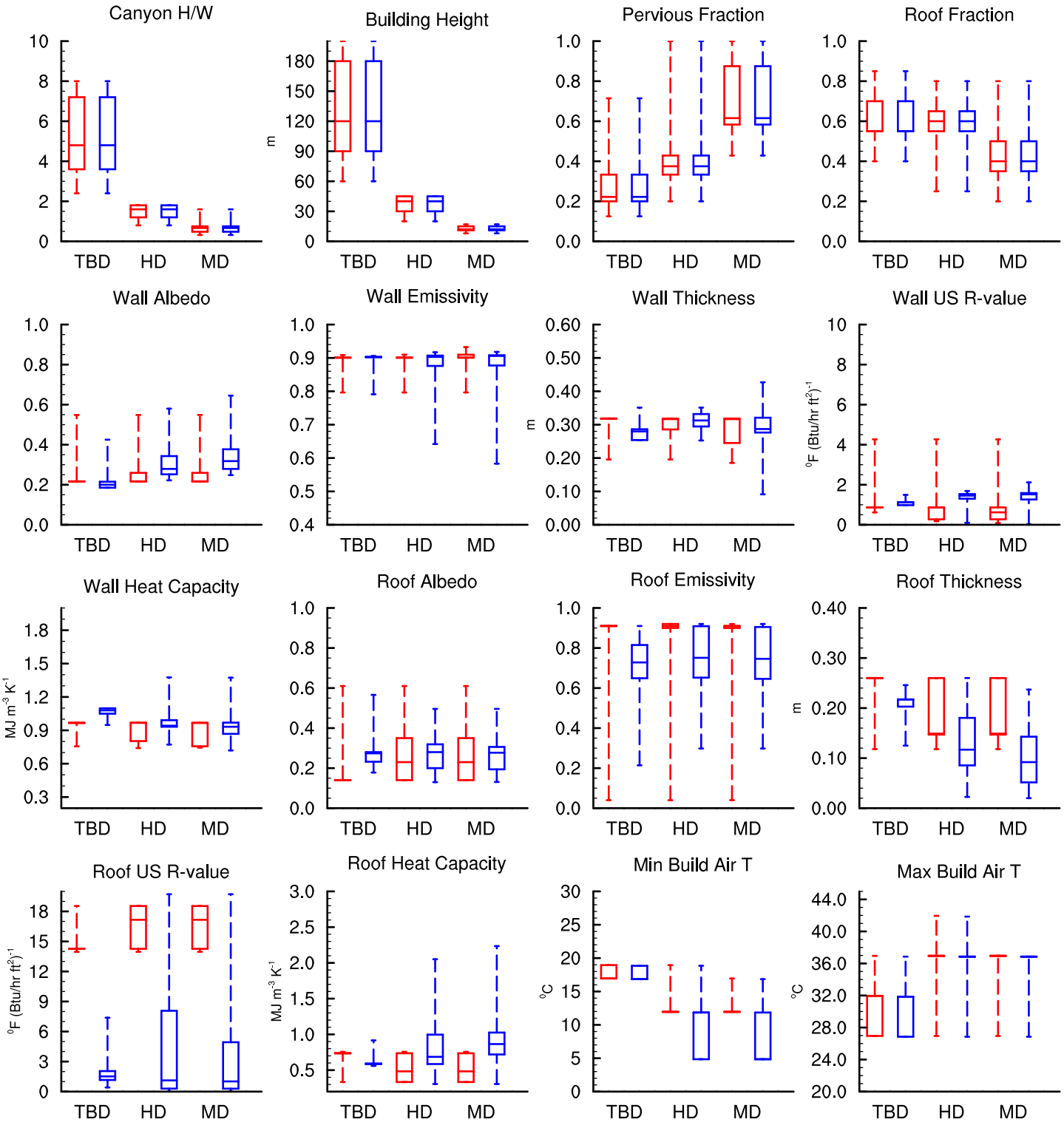

Figure 1. Boxplots of urban properties for thirty-three regions and three density classes; tall building district (TBD), high density (HD), and medium density (MD). Red boxplots refer to the new urban properties data V2, while blue boxplots are for V1. Boxplots show median (middle horizontal bar), 75th and 25th percentiles (top and bottom horizontal bars), and at top and bottom, the maximum and minimum values. H/W = building height/street width.

dataset. The *mksurfdata_map* tool ingests this data and other data describing the land surface to generate a CLM surface dataset at climate model resolutions (e.g., the nominal resolution for CESM2 is 0.9375° latitude by 1.25° longitude).

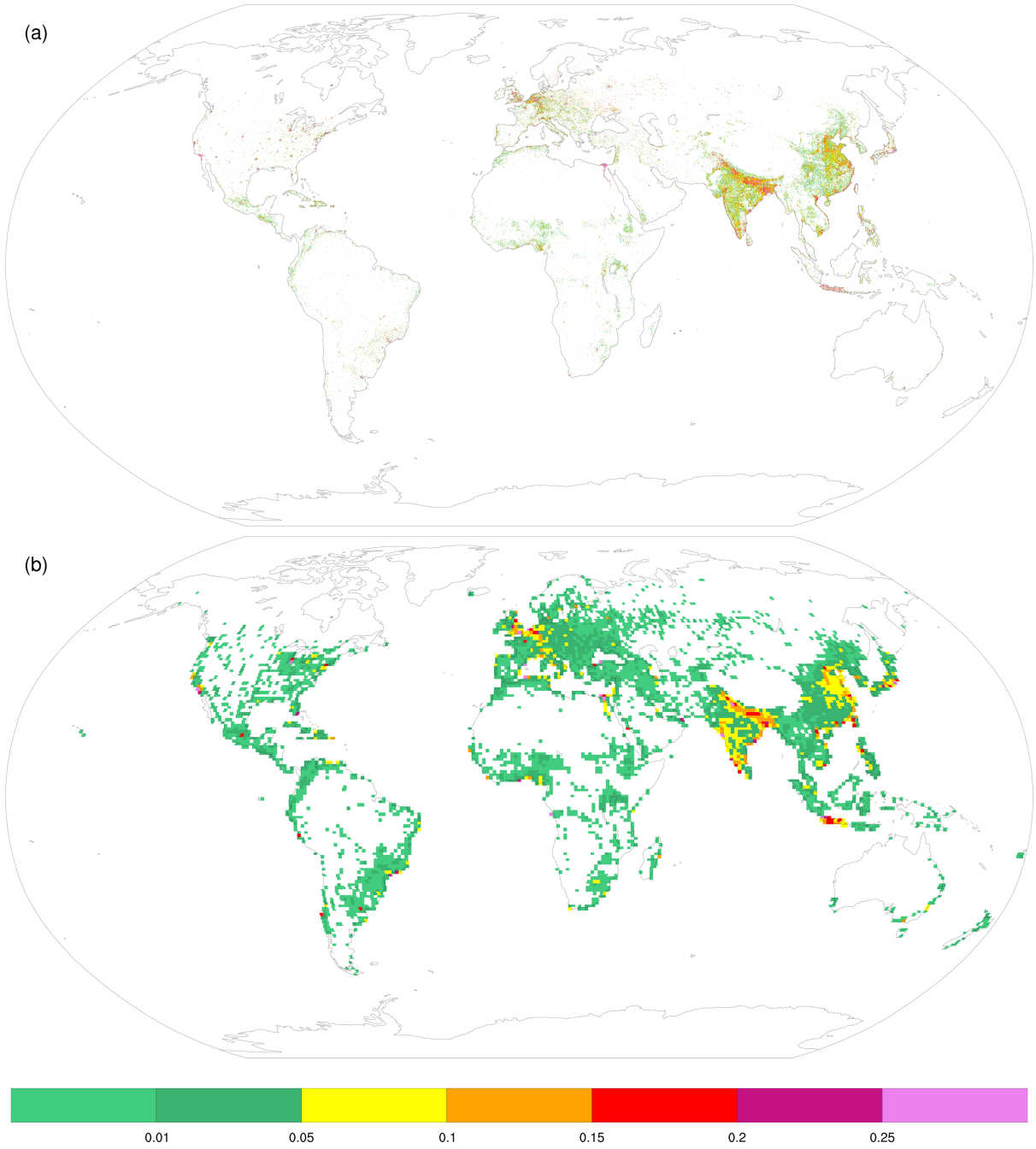

Figure 2. Urban fraction at a) 0.05° latitude by 0.05° longitude spatial resolution, b) CESM nominal resolution of 0.9375° by 1.25°.

Figure 2a shows total urban fraction of the TBD, HD, and MD classes at 0.05° by 0.05° resolution. As noted in J2010, the U.S. shows less urban area because of the omission of the LD class compared to regions like India and China where the dataset aggregates relatively small but high-frequency urban centers, like villages that have high population densities. Total urban extent is 835,823 km^2 or about 0.65% of the total global land area (excluding Antarctica and Greenland), with TBD, HD, and MD making up 0.0005%, 0.13%, and 0.52% of global land area. Schneider et al. (2009) notes that global urban extent maps that have emerged recently all suffer from scale-related limitations and definitional issues resulting in significantly different estimates of urban area. The estimate here is within the range reported by Schneider et al. (2009) (276,000 – 3,524,000 km^2). Figure 2b shows percent urban cover at the standard CESM2 resolution. A substantial percentage of land gridcells have at least one urban landunit (20%).

4. Space heating and air conditioning submodel

Heat produced by anthropogenic activities is small when distributed globally (0.028 W m^{-2} in 2005; Flanner, 2009), however, it can be a significant part of the local energy budget within cities that contributes to the UHI and thus should be accounted for within urban models. Sources of anthropogenic heat flux (AHF) include human metabolism, vehicles, commercial and residential buildings, industry, and power plants (Sailor, 2011). Of these sources, building space heating and air conditioning (HAC) is of particular relevance to a global climate model because HAC varies strongly with climate (Hadley et al., 2006).

Buildings account for over 33% of primary energy consumption globally of which nearly 60% is consumed by space heating and cooling together with water heating (IEA, 2011, 2013). Thus, an upper estimate of global primary energy consumption related to HAC is about 3.1 TW based on total primary energy consumption of 15.4 TW in 2005 [U.S. Energy Information Administration (EIA) (http://www.eia.doe.gov/emeu/iea). In the U.S., buildings account for about 40% of energy demand (EIA, 2012) of which 37-44% was used for HAC in residential and commercial buildings (EIA, 2009, 2008). In colder climates such as Europe, the energy demand for heating is higher while demand for cooling is relatively small (about 1% of total energy demand). About 48% of the total energy consumed in Europe is used for the generation of heat. Of this, 70% is used for low-temperature heat with about 70% of this attributable to space heating (European Technology Platform, 2011).

As discussed in Oleson (2012), the amount of anthropogenic heat added to the climate system due to HAC processes in CLMU4 is about 6.2 TW for present day, double the estimated actual value. The bias in simulated anthropogenic heat would be even larger if it wasn't for the fact that the method used to approximate the interior building temperature ends up being a net sink of energy from the perspective of the climate system (Oleson, 2012). This comes about due to the use of a weighted average of the interior roof and wall surface temperatures as an approximation of the interior building temperature instead of a more realistic interior building air temperature. If AHF is calculated without this energy sink term (as the sum of space heating and wasteheat only since the net air conditioning flux is zero), the present day AHF is 11.3 TW which is too high by a factor of almost four compared to observations (Oleson, 2012). The development of a new building energy model for CLMU was thus deemed to be a high priority, the main objective being to obtain a reasonable simulation of total energy due to building heating and air conditioning regionally and globally.

The main design objectives for the new building energy model are to: 1) provide a more realistic interior building air temperature that can be used to assess human thermal comfort; 2) account for the main processes influencing interior building air temperature and therefore heating and air conditioning demand; and 3) better balance energy within the building and thus in the urban system. It is important to recognize that the building energy model must be simple enough to operate globally and within the constraints of the available data provided by the urban properties dataset.

Sophisticated building energy models (BEMs) have recently been developed for urban models coupled to mesoscale climate models. Kikegawa et al. (2003) developed a Building Energy Analysis Model coupled to an urban canopy model that treats a building as a single thermal zone. Heating and cooling loads in the building are calculated for sensible and latent heat components. Sensible heat load is a function of the heat exchange between walls and indoor air, the transmission of solar radiation through the windows, sensible heat exchange through ventilation, and internal generation of heat from equipment and occupants. For latent heat load, the water vapour exchange through ventilation and evaporation from occupants is considered. The influence of the thermal storage of interior structures such as furniture and inner walls is accounted for by including them in the overall heat capacity of the indoor air. The BEM was able to reproduce the temporal variations of the outdoor and indoor air temperature in the central business district of Tokyo under conditions requiring air conditioning.

Salamanca et al. (2010) also developed a BEM that accounts for sensible heat exchange between windows and indoor air, and between walls, roof, and floor and indoor air, natural ventilation, and heat generation due to occupants and equipment. Water vapour mixing through ventilation and evaporation from occupants is considered for latent heat. The BEM also considers buildings of several floors with the indoor air temperature and moisture estimated for each floor. An energy budget equation is solved for indoor and outdoor surfaces considering heat diffusion and shortwave and longwave radiation interactions. Windows are treated explicitly in terms of both surface temperature and direct and diffuse solar radiation transmitted through

the window and reaching the indoor surface of the floor and walls. Heating and air conditioning loads are calculated based on keeping the indoor air temperature within a range of comfort defined by the user. The loads are also restricted by the maximum power of the HAC system.

Bueno et al. (2012) improved upon the Kikegawa et al. (2003) and Salamanca et al. (2010) BEMs by considering realistic, in addition to idealized, HAC systems, as well as passive building systems such as natural ventilation (treated similarly to infiltration) and window shades. The model considers a single thermal zone with an internal thermal mass representing the thermal inertia of the construction materials inside a building (e.g., separation between building levels) and assumes an adiabatic ground floor. The BEM is coupled to the Town Energy Balance (TEB) model (Masson, 2000). Pigeon et al. (2014) recently extended the evaluation of this BEM by comparing it to the EnergyPlus building energy model for five building types in European urban areas.

These BEMs perform well for case studies in which either individual building or neighbourhood-scale energy fluxes are simulated and the many input parameters are either well-defined or can be estimated by inference from site-level observations. While these models show great promise for modeling local building energy balances, their input parameters are too numerous and detailed to be effective for global applications as intended for the CESM. However, the BEMs have been used here to guide development of a building energy model within the CLMU that meets the design objectives stated above.

The BEM presented here (Figure 3) accounts for

- Conduction of heat through building surfaces (roof, sunlit and shaded walls, and floor)
- Convection (sensible heat exchange) between interior surfaces and indoor air
- Longwave radiation exchange between interior surfaces
- Ventilation (natural infiltration and exfiltration)

The BEM assumes a single thermal zone consistent with Bueno et al. (2012). Idealized HAC systems are assumed where the system capacity is infinite and the system supplies the amount of energy needed to keep the indoor air temperature within the specified limits at the time step of the model. A number of other processes are neglected here, not necessarily because they are not important but because of lack of data required to represent them in a global model. They could be easily added using the current BEM framework if data became available. Explicit treatment of windows in terms of their influence on indoor air temperature due to solar radiation transmission and thermal properties is neglected. This implies that space heating in winter will likely be overestimated and air conditioning in summer underestimated (Sailor, 2011). However, the effects of windows on the overall heat transfer properties of walls are accounted for (section 5). The thermal inertia of construction materials inside the building and internal heat gains due to occupants and equipment are also neglected. The thermal inertia of interior materials is likely to affect the diurnal cycle of indoor air temperature while internal heat gains likely have effects similar to windows (overestimating heating in winter and underestimating air conditioning in summer). Despite a lack of data regarding building floors in the J2010 data, a floor is essential for conserving longwave radiation within the building. An adiabatic ground floor (the surface of the building in contact with the ground is assumed to be well-insulated) made of a 0.1m thick slab of concrete is added consistent with Bueno et al. (2012) (but see section 8.2 for an assessment of the model's sensitivity to this assumption).

An energy balance is constructed for each interior surface and indoor air as

$$F_{rd,roof} + F_{cv,roof} + F_{cd,roof} = 0 \tag{1}$$

$$F_{rd,sunw} + F_{cv,sunw} + F_{cd,sunw} = 0 \tag{2}$$

$$F_{rd,shdw} + F_{cv,shdw} + F_{cd,shdw} = 0 \tag{3}$$

$$F_{rd,floor} + F_{cv,floor} + F_{cd,floor} = 0 \tag{4}$$

$$V_B \rho C_p \frac{\partial T_{iB}}{\partial t} - \sum_{sfc} A_{sfc} h_{cv,sfc} \left(T_{ig,sfc} - T_{iB}\right) - \dot{V}_{vent} \rho C_p \left(T_{ac} - T_{iB}\right) = 0 \tag{5}$$

where F_{rd} is the net longwave radiation (W m^{-2}), F_{cv} is the convection flux (sensible heat flux), and F_{cd} is the heat conduction flux (W m^{-2}) for each surface. In Eq. (5), V_B is the volume of building air (m^3), ρ is the density

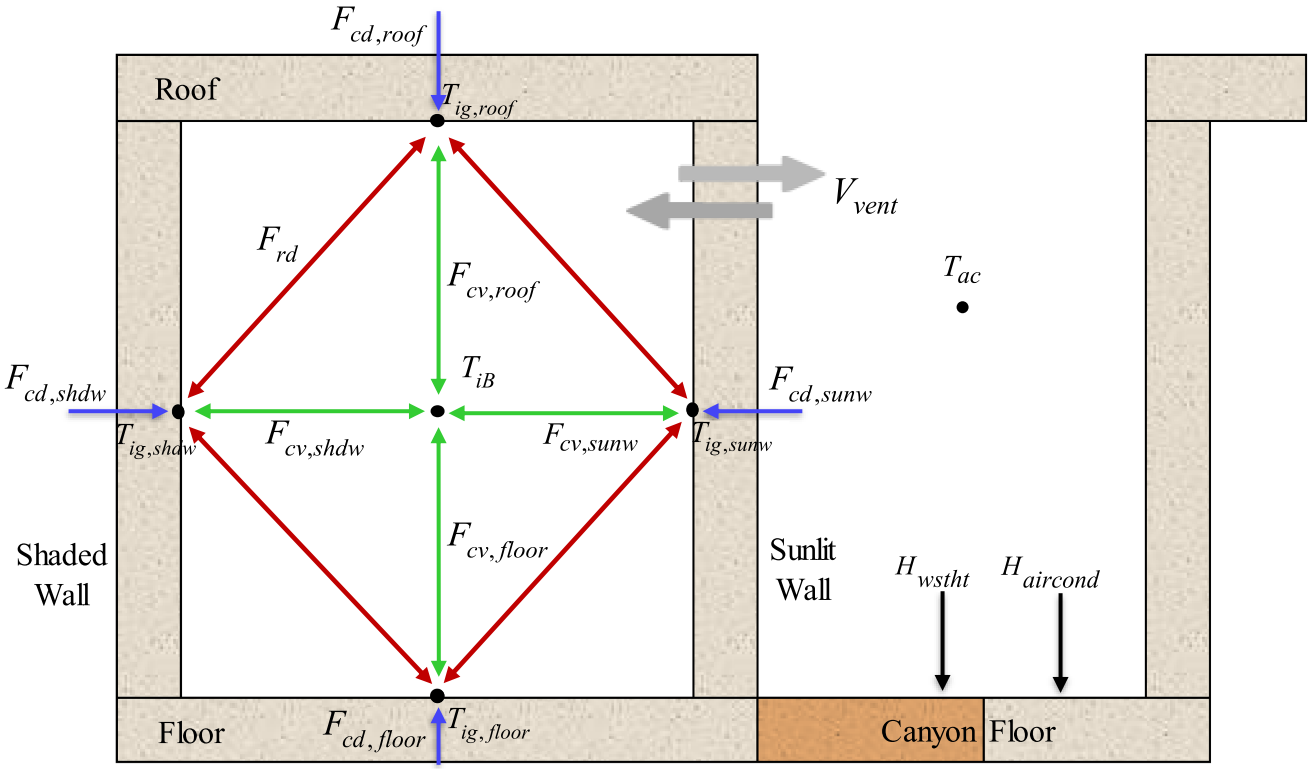

Figure 3. Schematic of building energy model. Blue arrows represent heat conduction fluxes (W m^{-2}) through the roof ($F_{cd,roof}$), walls ($F_{cd,sunw}$,$F_{cd,shdw}$), and floor ($F_{cd,floor}$). Green arrows represent convection (sensible heat transfer, W m^{-2}) between roof ($F_{cv,roof}$), walls ($F_{cv,sunw}$,$F_{cv,shdw}$), floor ($F_{cv,floor}$), and indoor air at temperature T_{iB} where $T_{ig,roof}$, $T_{ig,sunw}$, $T_{ig,shdw}$, $T_{ig,floor}$ are the interior surface temperatures of roof, walls, and floor. Red arrows represent radiation (longwave) exchange between interior surfaces (F_{rd}). V_{vent} is the ventilation flow rate (m^3 s^{-1}), T_{ac} is the urban canopy air temperature (K), H_{wstht} is the wasteheat resulting from inefficiencies in the heating and air conditioning equipment and from energy lost in the conversion of primary energy sources to end use energy (W m^{-2}), and $H_{aircond}$ is the heat removed from the interior of the building due to air conditioning (W m^{-2}).

of dry air at standard pressure P_{std} and indoor air temperature T_{iB} ($\rho = P_{std}/R_{da}T_{iB}$ where $P_{std} = 101325$ Pa and $R_{da} = 287.04$ J K^{-1} kg^{-1} is the dry air gas constant), $C_p = 1.00464 \times 10^3$ is the specific heat of dry air (J kg^{-1} K^{-1}), A_{sfc} is the area (m^2), $h_{cv,sfc}$ is the convective heat transfer coefficient (W m^{-2} K^{-1}), and $T_{ig,sfc}$ is the interior surface temperature of each surface (subscript *sfc* is roof, sunw, shdw, or floor). The last term in Eq. (5) represents exchange of indoor air and outdoor air in the urban canyon where $\dot{V}_{vent}$ is the ventilation air flow rate (m^3 s^{-1}) (an adjustable parameter) and T_{ac} is the urban canopy layer air temperature (K).

Due to a lack of reliable global data on building width for these urban density types, we assume that building width is equal to street width W (m). Then, for building depth of 1 m and since $V_B = WH$ (m^3), $A_{roof} = A_{floor} = W$ (m^2), and $A_{sunw} = A_{shdw} = H$ (m^2), where H is building height (m), Eq. (5) can be rewritten as

$$H\rho C_p\frac{\partial T_{iB}}{\partial t} - h_{cv,roof}\left(T_{ig,roof} - T_{iB}\right) - h_{cv,floor}\left(T_{ig,floor} - T_{iB}\right) - \frac{H}{W}h_{cv,sunw}\left(T_{ig,sunw} - T_{iB}\right) - \frac{H}{W}h_{cv,shdw}\left(T_{ig,shdw} - T_{iB}\right) - \left(\frac{ACH}{3600}\right)H\rho C_p\left(T_{ac} - T_{iB}\right) = 0 \quad (6)$$

where ventilation is represented by *ACH*, the number of air exchanges between indoor and outdoor volume of air per hour. $ACH = 0.3$ [at the lower end of the range given by Sailor (2011)] but see section 8.2 for sensitivity of the model to this assumption.

The longwave radiation fluxes are derived by linearizing the longwave radiation equations using a Taylor series expansion and assuming one reflection from each surface. An example of the set of linearized net longwave radiation equations for the roof (ceiling) is shown in the supporting information (Text S1).

The convective heat flux, e.g., for the roof is

$$F_{cv,roof} = h_{cv,roof}\left(T^{t+1}_{ig,roof} - T^{t+1}_{iB}\right) \tag{7}$$

where $h_{cv,roof}$ is the convective heat transfer coefficient for the roof to indoor air (W m^{-2} K^{-1}). The convective heat transfer coefficients are from the simple natural convection algorithm in EnergyPlus (EnergyPlus, 2012) consistent with Bueno et al. (2012). For a vertical surface (walls), $h_{cv,sunw} = h_{cv,shdw} = 3.076$ W m^{-2} K^{-1}; for a horizontal surface with reduced convection (i.e., a roof with $T_{ig,roof} > T_{iB}$ or a floor with $T_{ig,floor} < T_{iB}$), $h_{cv,roof} = h_{cv,floor} = 0.948$ W m^{-2} K^{-1}; for a horizontal surface with enhanced convection (i.e., a roof with $T_{ig,roof} \le T_{iB}$ or a floor with $T_{ig,floor} \ge T_{iB}$), $h_{cv,roof} = h_{cv,floor} = 4.040$ W m^{-2} K^{-1}.

The conduction flux is solved by using the Crank-Nicholson method, which combines the explicit method with fluxes evaluated at time t and the implicit method with fluxes evaluated at time t+1. The conduction flux from the innermost surface layer node depth $z_{i=N_{levurb}}$ to the interior surface $z_{h,i=N_{levurb}}$, e.g., for the roof is

$$F_{cd,roof} = \alpha\frac{\lambda\left[z_{h,i=N_{levurb}}\right]\left(T^{t+1}_{ig,roof} - T^{t+1}_{i=N_{levurb}}\right)}{z_{h,i=N_{levurb}} - z_{i=N_{levurb}}} + (1-\alpha)\frac{\lambda\left[z_{h,i=N_{levurb}}\right]\left(T^{t}_{ig,roof} - T^{t}_{i=N_{levurb}}\right)}{z_{h,i=N_{levurb}} - z_{i=N_{levurb}}} \tag{8}$$

where $\alpha = 0.5$, $\lambda\left[z_{h,i=N_{levurb}}\right]$ is the thermal conductivity (W m^{-1} K^{-1}) of layer $i = N_{levurb}$, $T^{t}_{i=N_{levurb}}$ is the temperature (K) of layer $i = N_{levurb}$ obtained from the solution of the heat transfer equations at time t, and $z_{h,i=N_{levurb}} - z_{i=N_{nlevurb}}$ is one-half the thickness of layer $i = N_{levurb}$ (m) (Oleson, Bonan, et al., 2010). An additional minor change to the model is that the number of layers used to represent heat conduction in roofs and walls in CLMU4 had been constrained to be the same as the number of ground layers in CLM4 ($N_{levurb} = 15$). Here, that restriction has been removed and ten layers ($N_{levurb} = 10$) are now used to represent roofs and walls which represents a reasonable compromise between representing heat transfer and computational savings (section 5).

The multi-layer column is not used for the floor, instead, Eq. (4) is rewritten as

$$\Delta z_{floor} C_{p_{floor}} \frac{\partial T^{t+1}_{ig,floor}}{\partial t} + F_{rd,floor} + h_{cv,floor}\left(T^{t+1}_{ig,floor} - T^{t+1}_{iB}\right) = 0 \tag{9}$$

where $\Delta z_{floor} = 0.1$ m is the floor thickness and $C_{p_{floor}} = 2.068$ MJ m^{-3} K^{-1} is the volumetric heat capacity of a concrete floor (Salamanca et al., 2010).

The linear system of five equations (Eqs. (1)-(5)) and five unknowns (T^{t+1}_{iB}, $T^{t+1}_{ig,roof}$, $T^{i+1}_{ig,sunw}$, $T^{t+1}_{ig,shdw}$, $T^{t+1}_{ig,floor}$) are solved using the LAPACK routine DGESV (http://www.netlib.org/lapack).

If $T^{t+1}_{iB} > T_{max}$ or $T^{t+1}_{iB} < T_{min}$ where T_{max} and T_{min} are the maximum and minimum indoor air temperatures prescribed by the J2010 urban properties dataset, the energy required to decrease (air conditioning) or increase (space heating) the indoor air temperature is calculated as

$$F_{cool} = \frac{H\rho C_p}{\Delta t}\left(T^{t+1}_{iB} - T_{max}\right) T^{t+1}_{iB} > T_{max} \tag{10}$$

$$F_{heat} = \frac{H\rho C_p}{\Delta t}\left(T_{min} - T^{t+1}_{iB}\right) T^{t+1}_{iB} < T_{min} \tag{11}$$

where Δt is the model time step (s). The indoor air temperature is then reset to T_{max} or T_{min}.

Wasteheat factors that account for inefficiencies in the heating and air conditioning equipment and from energy lost in the conversion of primary energy sources to end use energy are derived from Sivak (2013). In that analysis the energy demand for space heating and air conditioning E_{demand} was derived from site energy E_{site}, the average efficiency of cooling and heating appliances COP (coefficient of performance), and power plant efficiency P_{eff}

$$E_{demand} = E_{site}/COP/P_{eff} \tag{12}$$

Heating and air conditioning COP are assumed to be 0.9 and 3.6, respectively. The weighted efficiencies of power plants for generating energy used for heating and cooling buildings were calculated to be 0.96 and

0.43, respectively (Sivak, 2013). Thus, E_{demand} for space heating and cooling is $1.2E_{site}$ and $0.6E_{site}$, respectively. Here, E_{site} is taken to be F_{cool} and F_{heat} from Eqs. (10) and (11). The wasteheat H_{wstht} is therefore derived as $0.2F_{heat}$ for heating (since one unit of energy was already used to heat the building interior) and $0.6F_{cool}$ for air conditioning (since the energy consumed is used to transfer heat from the building interior to the exterior). The wasteheat factors in the previous version of the model for heating and cooling were much higher at 1.33 and 4.0, respectively. The analysis by Sivak (2013) is based on efficiencies of heating and cooling appliances and power plants and energy source distributions in the U.S. but was applied globally here for simplicity. The model could be improved for other regions if these factors were known. The heat removed by air conditioning $H_{aircond} = F_{cool}$ and the wasteheat H_{wstht} are added as sensible heat to the canyon floor as in CLMU4 (Oleson, Bonan, et al., 2010). The total anthropogenic heat flux released into the climate system due to space heating and air conditioning in CLMU5 is

$$AHF = F_{heat} + H_{wstht} \tag{13}$$

In the next section, an urban properties tool and improvements in the urban properties data are described.

5. New urban properties tool and data

The Excel spreadsheet that was produced by J2010 to generate urban properties for CLMU was unwieldy and prone to errors particularly when trying to make modifications or develop future urban development scenarios. The spreadsheet has been replaced by an urban properties tool consisting of several NCAR Command Language (NCL) programs which are executed in sequence by a a c-shell driver script (Figure 4). Input to the NCL programs is in the format of comma separated value (csv) files, keyword/value text files, and NetCDF files. The new urban properties tool is available as part of the Toolbox for Human-Earth System Integration & Scaling (THESIS) tool set (http://www.cgd.ucar.edu/iam/projects/thesis/thesis-urbanproperties-tool.html; Feddema & Kauffman, 2016).

The driver script (*urban_prop.csh*) specifies three input csv files (by default, *mat_prop.csv*, *lam_spec.csv*, and *city_spec.csv*) that describe the morphological, radiative, and thermal properties of urban areas (Figure 4). This is combined with urban extent data from J2010 to generate a global urban extent dataset at 0.05° latitude by longitude combined with a set of urban properties dimensioned by urban density class and region in NetCDF format (*urban_properties_data.05deg.nc*).

The *mat_prop.csv* file describes the fundamental thermal and radiative properties of materials typically used in urban construction. These properties are used in *lam_spec.csv* to construct walls (including windows and frames), roofs, and roads. The *city_spec.csv* file assigns the wall, window, roof, and road types to each of the four urban density classes for thirty-three global regions. Morphological properties (building height, height to street width ratio, pervious canyon floor fraction) are also assigned within this file. A *region_prop.csv* file containing the morphological, radiative, and thermal properties associated with each of the four urban density classes within each of the thirty-three regions is output at this point.

After the *region_prop.csv* file is created, the driver script executes an NCL program (*gen_data_1km.ncl*) which combines the properties data with 1km urban extent data from J2010 (*tall_bldg_dist_1km.nc, high_dens_1km.nc, med_dens_1km.nc* in Figure 4) to generate a NetCDF file of global urban properties dimensioned by urban density class (TBD, HD, and MD; the LD class is dropped at this point) and region, and urban extent data gridded at 1km spatial resolution. Next, the driver executes an NCL program (*gen_data_05deg.ncl*) which aggregates the 1km data into a 0.05° dataset in NetCDF format suitable for ingestion by the CLM *mksurfdata_map* tool (https://escomp.github.io/ctsm-docs/doc/build/html/users_guide/using-clm-tools/index.html). The *mksurfdata_map* tool creates a CLM surface dataset at the desired climate model resolution (e.g., *surfdata_0.9x1.25_simyr2000.nc* in the example shown in Figure 4). The percentages of urban extent for the TBD, HD, and MD urban classes are explicitly specified for each climate model grid cell, while the urban properties are specified by urban density class and region. The surface dataset is read in by CLM at run time and the properties data are assigned to specific grid cells and urban density classes according to the region that the grid cell falls within.

Finally, a standalone NCL routine (*gen_data_clm.ncl*; not shown in Figure 4) can be run separately after the *mksurfdata_map* tool creates the CLM surface dataset. This creates a supplementary file of setpoints for the

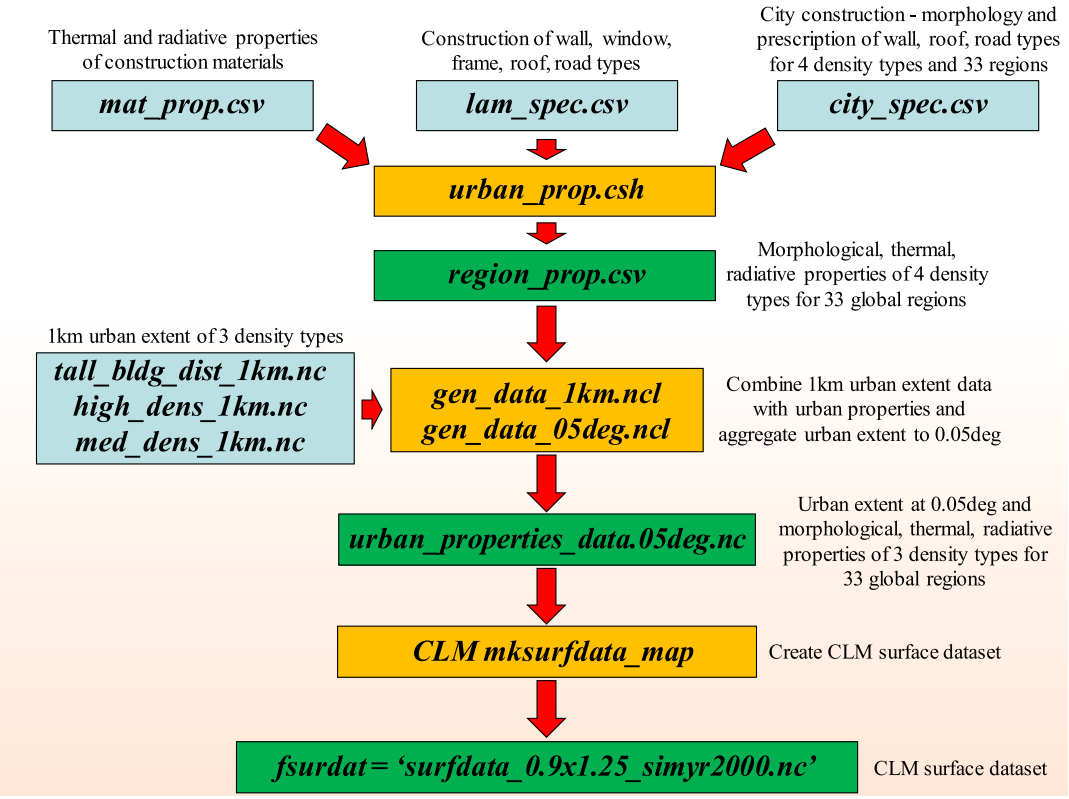

Figure 4. Schematic of THESIS urban properties tool. Executable scripts are in orange, input files are blue, and output files are green. See section 5 for more details.

maximum interior building temperature at yearly time resolution. This is desirable for transient simulations in which air conditioning may not be available (e.g., before circa 1950). The urban properties tool was first verified as able to reproduce the original J2010 data within roundoff and then the csv files were modified as follows for the new version of the urban properties dataset.

As noted in section 4, the simulated present day AHF is too high in CLMU4 compared to observations, indicating that heat transfer between building exterior and interior may be overestimated. Recent CLMU simulations of tower sites in Helsinki, Finland, which used the default properties specified by J2010, also indicated similar problems (Karsisto et al., 2015). Since heat transfer is mainly controlled by the thermal properties of roofs and walls, these properties as specified by J2010 were reassessed. Another issue identified is that final wall properties for thermal conductivity/resistance were calculated by averaging total wall resistance (based on treating wall layers in series) for the wall cavity, wall bridging and glass areas, then treating these facets in parallel. These total wall values were then distributed equally to all layers of the model walls. However, by averaging total wall properties in this way, heating and cooling rates across the walls can be distributed unrealistically. For example, for a wall with brick exterior and drywall/insulation interior, the resulting values for thermal conductivity were generally too low for the exterior wall layers where much of the heat exchange with the urban canopy takes place and too high for the interior wall layers where heat transfer into the building interior occurs. Similarly the weighted average wall heat capacities were also spread through all layers of the wall, often providing unrealistic wall layer heat capacity properties.

To correct these potential biases and to improve the ability to construct more realistic scenarios of building types, the dataset has been modified so that each wall facet (wall cavity, wall bridge, window pane and window frame) is represented by 10 layers assigned to a specific material type. For some wall types all 10 layers can be identical (e.g., corrugated metal), for other walls, layers can be variable with several layers representing external wall materials (e.g., bricks or siding), interior wall insulation, and interior wall finishes such as plaster board. We still average the final heat capacity (depth and area weighted) and thermal conductivity (as parallel surfaces) for each layer across the entire wall from the four facets. This change results in more realistic energy absorption and storage characteristics associated with different wall types. For high latitude

Table 1
Tower site information. Frequency (minutes) is the frequency of observed and model data. CLMU5 simulations for these sites are compared to the previous simulation results referenced here as described in section 7.1. Model/Data differences from the previous simulations include differences in the hydrology of the pervious canyon floor (all sites), the new BEM (all sites), addition of wasteheat (Tou04), and the replacement of J2010 wall/roof materials with the new urban properties data (Hotel Torni). Two CLMU5 simulations are run for Hotel Torni, one with the old BEM and new wall/roof properties and one with the new BEM and new wall/roof properties.

Tower Site	Location	Evaluation Time Period	Frequency	Previous Simulation Results	Previous Parent CLM Version	Model/Data Differences
Me93	Mexico City, Mexico	2-7 Dec, 1993	60 min	Oleson, Bonan, Feddema, Vertenstein, and Grimmond (2008)	CLM3	hydrology, BEM
Vl92	Vancouver, Canada	13-25 Aug, 1992	60 min	Oleson, Bonan, Feddema, Vertenstein, and Grimmond (2008)	CLM3	hydrology, BEM
Pres04	Preston, Australia	15 Jan – 15 Nov, 2004	30 min	Grimmond et al. (2011)	CLM3.5	hydrology, BEM
Tou04	Toulouse, France	15 Apr, 2004 – 15 Feb, 2005	30 min	Demuzere et al. (2013)	CLM4	hydrology, BEM, wasteheat
Hotel Torni	Helsinki, Finland	9 Jan – 31 Dec, 2012	60 min	Karsisto et al. (2015)	CLM4	hydrology, BEM, wall/roof materials

locations, insulation was added to walls to alleviate the deficiencies noted in Karsisto et al. (2015) (section 7.1). The J2010 dataset as implemented in CLM4 also used a weighted average of the properties of three building types within each density class, which resulted in building properties not directly traceable to real materials. Here, we simply use the properties of the dominant building type by area for each density class and region.

The current version of the dataset retains the fundamental building types, with a few corrections, created in J2010. Although generally similar, the current implementation should lead to different urban temperature and building energy characteristics compared to simulations using the J2010. The characteristics of the new urban properties data (V2) compared to the original created by J2010 (V1) is summarized in the box plots of Figure 1. Urban morphology (canyon height to width, building height, pervious and roof fractions) are unchanged from V1 but are shown for completeness. Some small changes in the values of wall and roof albedo and emissivity are evident that are primarily due to the use of a single building type within each density class instead of the mixture of types that was used in V1. This results in less spatial variability in these quantities as well with the exception of the HD and MD roof albedos.

Instead of reporting the averaged thermal conductivities of walls and roofs, we calculated U.S. R-values [ratio of the temperature difference across an insulator, i.e., a wall or roof) and the heat flux (heat flow per unit area) through it; °F (Btu/hr ft^2)$^{-1}$]. The most significant changes in thermal properties are associated

Table 2
Key model parameters for the tower sites. H/W is the building height to street width ratio, W_{roof} is the roof fraction, and f_{prvrd} is the pervious fraction of canyon floor. Roof, wall, and road materials are used to derive values for thermal conductivity and heat capacity as described in the references provided in the table footnotes. Space heating is controlled by Tmin, the minimum interior building temperature thermostat setting. Wasteheat (W m^{-2}), when active, is $H_{wstht} = 0.2F_{heat}$ where F_{heat} is the energy required for space heating as described in section 4. Air conditioning is not simulated at any of the sites.

Tower Site	H/W	W_{roof}	f_{prvrd}	Roof Materials	Wall Materials	Road Materials	Thermostat Settings	Wasteheat
Me93[1]	1.18	0.55	0.04	asphalt roll, concrete/stone, insulation, gypsum	stone/window	asphalt, concrete, stone aggregate	None	Off
Vl92[1]	0.39	0.51	0.11	gravel, insulation, concrete	concrete	asphalt, concrete, stone aggregate	None	Off
Pres04[2]	0.42	0.445	0.68	metal, concrete, terracotta, asbestos cement	brick, softwood, concrete, asbestos cement, metal, hardwood, brick	asphalt, concrete	None	Off
Tou04[3]	1.4	0.54	0.21	red tiles, wood	red bricks	asphalt, stone aggregate, gravel	Tmin = 19°C	Active
Hotel Torni[4,5]	1.33	0.37	0.026	ceramic tile, plywood, insulation, drywall	brick clay, concrete, insulation, drywall	asphalt, concrete	Tmin = 19°C	Active

[1]Oleson, Bonan, Feddema, Vertenstein, and Grimmond (2008). [2]Grimmond et al. (2011). [3]Demuzere et al. (2013). [4]Karsisto et al. (2015). [5]Roof, wall, and road materials are from the new urban properties dataset as described in section 5.

Table 3
Parameter values for BEM sensitivity simulations as described in section 7.2. ACH is the number of air changes per hour, h_{cv} is the convective heat transfer coefficient, ε is emissivity, and Δz_{floor} is floor thickness.

BEM Input Parameter	Units	Default Value	Sensitivity Test Value(s)	Simulation
ACH	hr^{-1}	0.3	0.0, 0.5	ACH00, ACH05
h_{cv}	$W\ m^{-2}\ K^{-1}$	0.948-4.040	8.0	S2010
ε	-	0.9	0.8, 0.96	E80, E96
Δz_{floor}	m	0.1	0.3	FT03

with roofs (Figure 1). All three density classes have significantly larger R-values for roofs than in the V1 dataset. The lower R-values for the V1 roofs reflect the averaging of building types as well as averaging across individual layers. Walls are less affected by the averaging because of the presence of windows/frames in both datasets. The highest R-value walls are associated with a plaster veneer/brick masonry wall with double-pane windows. We note that accounting for the thermal properties of windows and window frames in the dataset significantly reduces the wall R-values. The median whole wall R-value without windows/frames is about 10. While maximum building interior air temperatures (controlling AC) are unchanged, minimum temperatures have been increased in V2 to more reasonable levels for HD and MD classes. These had been set to low levels in some regions to compensate for the unrealistic AHF in V1.

Further changes to the dataset reflect the need for scenario development, thus allowing for the creation of hypothetical wall types, and the easier interchange of wall facets (e.g. replacing single pane windows with double pane windows and replacing wall components). Further additions include three hypothetical walls for stylized scenarios, with one set representing well insulated walls and roofs with a high heat capacity exterior layer (40% of the exterior is brick or tile), a second wall and roof combination with high heat capacity interior materials covered by a well insulated exterior and interior high heat capacity mass (bricks), and a third type that represents well insulated walls with lightweight materials. The intent of these walls is that they can represent relatively cheap wall types that can be made from local materials [e.g., Rammed Earth walls (Kraus et al., 2013, 2015) or, for example, material roof tiles using sisal plants (Tonoli et al., 2011)], but at the same time walls that may present advantages with respect to energy conservation and human comfort in different regional climates. To further facilitate scenario development, some exterior wall and roof materials have been duplicated with albedo values of 0.15 and 0.85 to represent highly absorbing or highly reflecting facets.

The THESIS tool currently includes an example of a future urban development scenario that could be explored by a user of the model. This corresponds to a roof albedo experiment designed to reduce energy consumption, urban temperature, and human heat stress. In this scenario, the *mat_prop.csv*, *lam_spec.csv*, and *city_spec.csv* are modified such that existing roof albedos are replaced by higher or lower albedos as described above depending on region. Results from this scenario and others will be described in a future manuscript.

Table 4
Summary statistics of hourly simulated compared to observed net radiation (Q^*) and sensible heat (Q_H), latent heat (Q_E), and storage (Q_S) fluxes for Me93 for 2-7 Dec 1993. Values in parentheses are from the previous version of CLMU documented in Oleson, Bonan, Feddema, Vertenstein, and Grimmond (2008). $\overline{x}_{mod}$ is the model mean ($W\ m^{-2}$), $\overline{x}_{obs}$ is the observation mean ($W\ m^{-2}$), MBE is the mean bias error (model minus observations) ($W\ m^{-2}$), RMSE is the root-mean-square error ($W\ m^{-2}$), and R^2 is the coefficient of determination. The number of observations is 123.

	Q^*	Q_H	Q_E	Q_S
$\overline{x}_{mod}$	64 (68)	59 (63)	3 (3)	3 (3)
$\overline{x}_{obs}$	43	50	5	-11
MBE	21 (25)	9 (13)	-2 (-2)	14 (14)
RMSE	42 (44)	32 (34)	10 (10)	37 (36)
R^2	1.00 (0.99)	0.81 (0.81)	0.28 (0.28)	0.97 (0.96)

6. Heat stress indices module

Heat stress is a leading cause of human mortality in the U.S. and worldwide (CDC, 2006; Robine et al., 2008). Heat stress can be amplified by global scale warming and in urban areas because of the urban heat island effect. High levels of humidity and low wind speeds can combine with temperature extremes to exacerbate heat stress. In recognition of this, Buzan et al. (2015) developed a module of heat stress indices (four moist thermodynamic quantities and nine heat stress metrics) calculated online in CLM that can be used to assess human thermal comfort for rural and urban areas. These indices are calculated from combinations of simulated near-surface air temperature, humidity, and in some cases, wind speed. The heat stress indices module is fully described in Buzan et al. (2015) and is not discussed further here. An application of these metrics to a study of interactions between urbanization, heat stress, and climate change over the U.S. can be found in Oleson et al. (2015).

Table 5
As in Table 4 but for Vl92 for 13-25 August, 1992. Values in parentheses are from the previous version of CLMU documented in Oleson, Bonan, Feddema, Vertenstein, and Grimmond (2008) but reported for the entire period as in Grimmond et al. (2010) for phase 1 of the international urban energy balance model comparison project instead of the two periods used by Oleson, Bonan, Feddema, Vertenstein, and Grimmond (2008). The number of hourly observations is 312.

	Q^*	Q_H	Q_E	Q_S
$\bar{x}_{\mathrm{mod}}$	123 (128)	113 (119)	10 (8)	0 (1)
$\bar{x}_{obs}$	131	72	15	42
MBE	-8 (-3)	41 (47)	-5 (-7)	-42 (-41)
RMSE	28 (28)	67 (76)	18 (19)	69 (69)
R^2	0.99 (0.99)	0.85 (0.85)	0.35 (0.29)	0.87 (0.86)

7. Simulations

7.1. Flux tower simulations

Several urban flux tower sites have been used to evaluate past versions of the urban model in terms of its ability to reproduce urban energy and water fluxes, and surface and air temperatures (Demuzere et al., 2013; Grimmond et al., 2011; Karsisto et al., 2015; Oleson, Bonan, Feddema, Vertenstein, & Grimmond 2008). Even if changes to the urban model are not expected to significantly change the performance of the model in certain cases (as noted below), the urban model may still be responsive to changes in the CLM version in which it is embedded, mostly because the updated hydrology for each CLM version is implemented for the pervious canyon floor hydrology. Thus it is also important to periodically re-evaluate the urban model when the parent CLM version changes.

Here, five sites are simulated with CLMU5 (Table 1):

1. Me93: The historic city core of Mexico City, Mexico (Oke et al., 1999).
2. Vl92: A light industrial site in Vancouver, British Columbia, Canada (Grimmond & Oke, 2002; Voogt & Grimmond, 2000).
3. Pres04: A moderately developed low-density housing site in Preston, Australia (Coutts et al., 2007a, 2007b).
4. Tou04: The old city centre of Toulouse, France (Masson et al., 2008).
5. Hotel Torni: A dense city-centre site in Helsinki, Finland (Karsisto et al., 2015).

Table 1 lists references for simulations completed using previous versions of CLMU and their parent CLM version. The Me93, Vl92, Pres04, Tou04, and Hotel Torni simulations are repeated using CLMU5 and compared to these results reported previously.

The urban morphological, radiative, and thermal properties are still specified as in Oleson, Bonan, Feddema, Vertenstein, and Grimmond (2008) for the Me93 and Vl92 sites and Grimmond et al. (2011) for Pres04 (see Table 2 for a list of key parameters and building materials). Changes in model performance for these three sites will only be due to the new BEM and differences in the hydrological behaviour of the pervious canyon floor which follows the hydrology of its respective parent CLM versions (Table 1). For the Me93 and Vl92 sites, model performance is expected to be similar since the interior building temperature is not actively controlled by heating or air conditioning as consistent with the prior simulations and the pervious canyon floor fraction is small (Table 2). For the Pres04 site, the pervious canyon floor fraction is larger than the Me93 and Vl92 sites (Table 2) so differences in hydrology can have a larger effect. However, the interior building temperature is not actively controlled by heating or air conditioning as in Grimmond et al. (2011) so the BEM is not expected to have much effect.

For Tou04, differences will be due to the new BEM, pervious canyon floor hydrology, and the addition of wasteheat (Table 1). Unlike the Demuzere et al. (2013) simulation, the wasteheat from space heating is active in CLMU5 and is applied as a heat flux to the canyon floor (Table 1). As in Demuzere et al. (2013), the anthropogenic heat flux for Tou04 also includes the sum of a prescribed traffic flux plus the anthropogenic heat produced by the model due to space heating when the minimum interior building temperature is set to 19°C. The Tou04 site also provides an opportunity to evaluate the anthropogenic heat flux from the new BEM (Pigeon et al., 2007, 2008) and to perform sensitivity simulations for the BEM (section 7.2).

Karsisto et al. (2015) reported on a simulation for the Hotel Torni site in Helsinki, Finland. In this particular simulation, the J2010 data were used to specify the radiative and thermal parameters for the site instead of site-specific measured parameters. Here, we repeat the simulation for the Hotel Torni site, however, we now use the parameters from the new urban properties data described in section 5, which in this case are the same wall and roof types but with more realistic insulation conditions (Table 2). Thus, changes in model performance will be due to the new BEM, pervious canyon floor hydrology, and new wall/roof types (Table 1). An additional simulation without the new BEM is run to separate the effects of the new surface data from changes due to adding the new BEM.

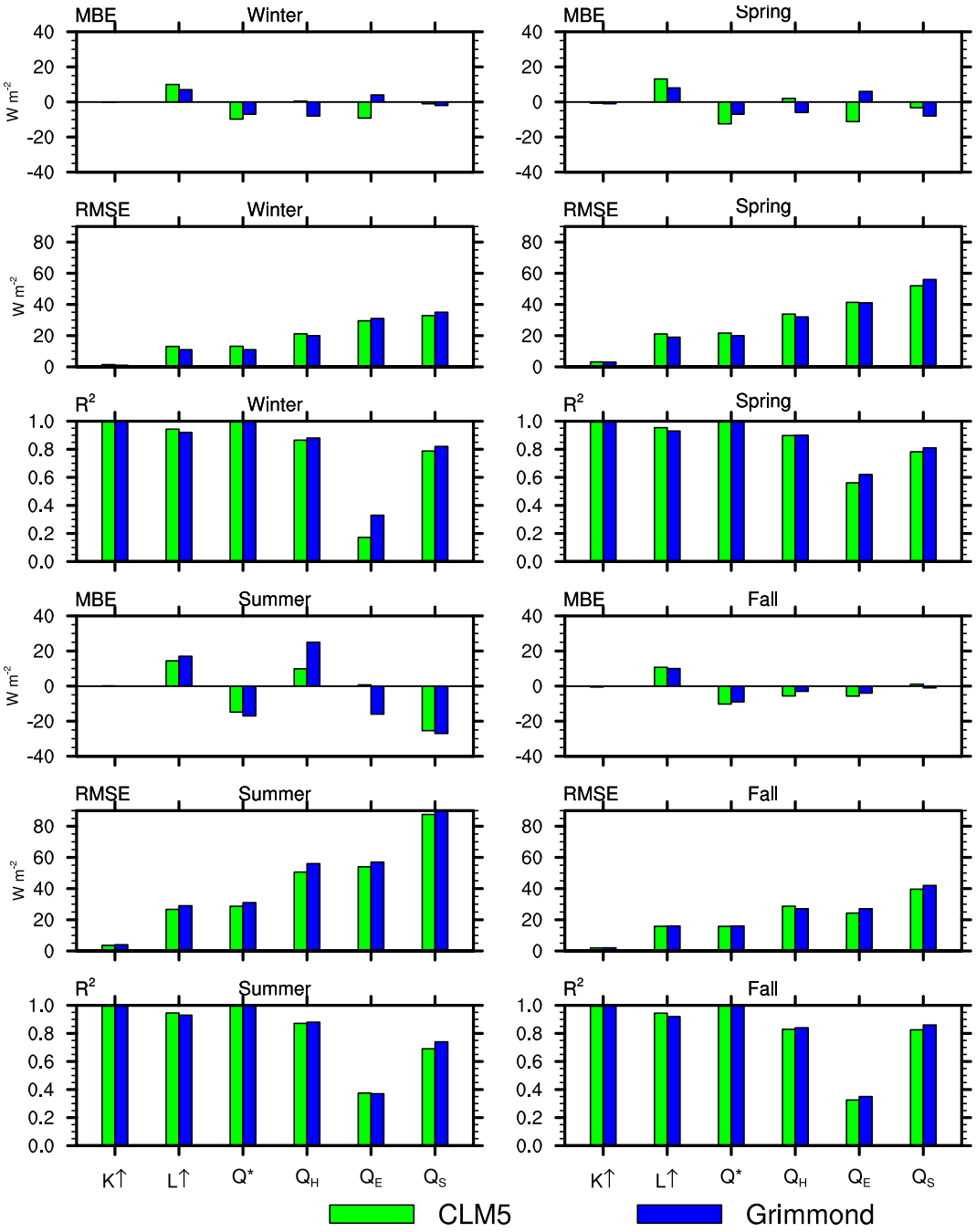

Figure 5. Summary statistics of half-hourly simulated compared to observed reflected solar radiation ($K\uparrow$), emitted longwave radiation ($L\uparrow$), net radiation (Q^*) and sensible heat (Q_H), latent heat (Q_E), and storage (Q_S) fluxes for Pres04 for four seasons. Winter is 15 July – 15 August, Spring is 15 October – 15 November, Summer is 15 January – 15 February, and Fall is 15 April – 15 May, 2004. Values denoted in blue are from the CLM simulation submitted to Grimmond et al. (2011). MBE is the mean bias error (model minus observations) (W m^{-2}), RMSE is the root-mean-square error (W m^{-2}), and R^2 is the coefficient of determination.

7.2. Sensitivity simulations

The Tou04 site, which offers both observed surface temperatures and energy fluxes including anthropogenic heat, is used to test the sensitivity of the model to the new input parameters that are associated with the BEM and subject to large uncertainties and variations among building types (Table 3). The new input parameters required by the BEM are the air changes per hour (*ACH*), the interior convective heat transfer coefficients

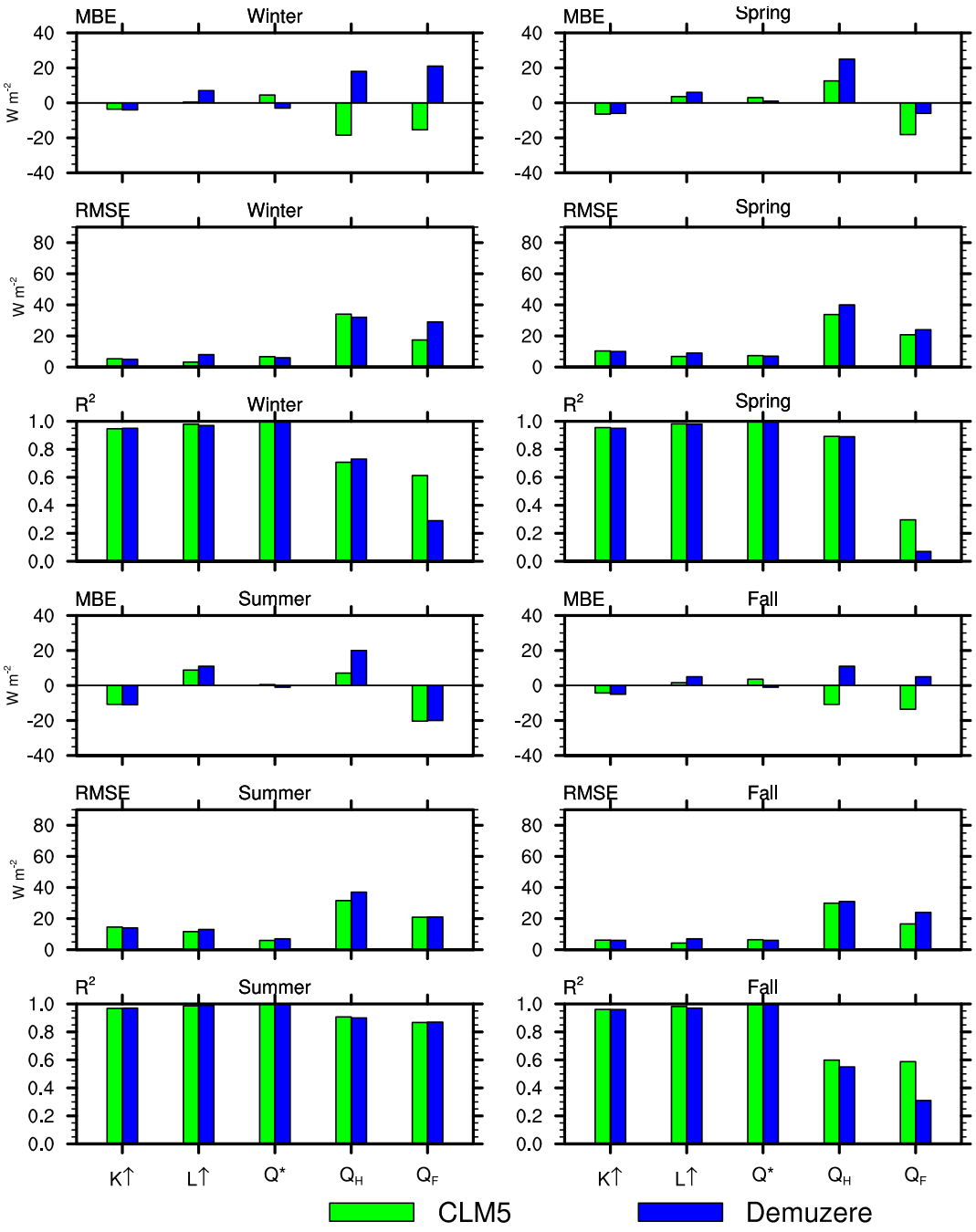

Figure 6. Summary statistics of half-hourly simulated compared to observed reflected solar radiation ($K\uparrow$), emitted longwave radiation ($L\uparrow$), net radiation (Q^*), sensible heat (Q_H), and anthropogenic heat (Q_F) fluxes for Tou04 for four seasons. Winter is 15 January – 15 February 2005, Spring is 15 April – 15 May 2004, Summer is 15 July – 15 August 2004, and Fall is 15 October – 15 November 2004. Values denoted in blue are from the CLM simulation reported in Demuzere et al. (2013). Note that the $K\uparrow$ values in parentheses are not always the same as in Table VI of Demuzere et al. (2013) because here any non-zero incoming solar radiation is set to a value of zero when the model sun is below the horizon. Statistics are described in Figure 5.

(h_{cv}), the emissivities of the interior surfaces (ε), and the thickness of the floor (Δz_{floor}). The baseline values for these are described in section 4 and listed in Table 3.

Sailor (2011) gives a range for ACH of 0.3 to 0.5. The model is thus also tested for a value of $ACH = 0.5$. The effect of eliminating ventilation completely is also tested ($ACH = 0.0$). These simulations are denoted as ACH05 and ACH00, respectively.

Table 6
Summary statistics of half-hourly simulated compared to observed surface temperatures of roof (T_{roof}), wall (T_{wall}), road (T_{road}), and canyon air (T_{canyon}) (K) for Tou04 for three seasons. Winter is 15 January – 15 February 2005, Summer is 15 July – 15 August 2004, and Fall is 15 October – 15 November 2004. Values in parentheses are from the CLM simulation reported in Demuzere et al. (2013). Statistics are described in Table 4.

	T_{roof}	T_{wall}	T_{road}	T_{canyon}
Winter				
MBE	1.6 (3.3)	0.1 (1.8)	-0.2 (-0.5)	-0.1 (0.2)
RMSE	2.5 (3.9)	0.4 (1.8)	1.0 (1.2)	0.4 (0.5)
R^2	0.89 (0.86)	0.99 (0.98)	0.92 (0.92)	0.99 (0.99)
Summer				
MBE	5.8 (5.9)	1.0 (1.5)	1.7 (1.8)	0.8 (0.9)
RMSE	6.5 (6.6)	1.2 (1.7)	2.6 (2.8)	1.1 (1.2)
R^2	0.92 (0.92)	0.97 (0.96)	0.96 (0.95)	0.97 (0.97)
Fall				
MBE	1.6 (2.5)	0.8 (1.7)	0.3 (0.2)	0.0 (0.2)
RMSE	2.4 (3.0)	1.0 (1.8)	1.4 (1.5)	0.3 (0.4)
R^2	0.92 (0.92)	0.99 (0.99)	0.95 (0.95)	0.99 (0.99)

Salamanca et al. (2010) used convective heat transfer coefficients for interior surfaces h_{cv} = 8 W m^{-2} K^{-1} which are quite different from the EnergyPlus coefficients used by the new BEM. A simulation denoted S2010 is conducted using this convective heat transfer coefficient for all interior surfaces.

The emissivity of interior surfaces of course depends on the type of surface. Interior surfaces of buildings are likely to be dominated by materials such as concrete, wood, metal, and drywall. However, it is reasonable to assume that most of the interior surface area of roofs and walls will be covered by some kind of paint. A reasonable range for the emissivity of paint, with the exception of aluminium paint and certain lacquers and varnishes, is 0.80-0.96 (Engineering Toolbox, 2014). Ground floor materials are likely to be dominated by wood, concrete, and carpet. Emissivities of these surfaces range from 0.85-0.95 (Engineering Toolbox, 2014). Simulations using the lower (ε = 0.80) and upper bounds (ε = 0.96) of these surfaces are denoted as E80 and E96, respectively. Building floors simulated in Salamanca et al. (2010) range up to 0.33 m in thickness, so a thicker concrete floor of Δz_{floor} = 0.3 m is also simulated here (denoted as FT03).

7.3. Global simulations

Global offline simulations (with CLM uncoupled from an active atmospheric model) at a nominal 1° spatial resolution (0.9375° latitude by 1.25° longitude) are conducted to exercise CLMU over a wide range of climatic conditions that are typically produced by the fully coupled CESM (as in Oleson (2012)). Simulations are run from 1850-2005 using atmospheric forcing (precipitation, incoming solar and longwave radiation, and air temperature, humidity, wind, and CO_2 concentration at the lowest atmospheric model layer) from a CCSM4 20th century ensemble member (Gent et al., 2011) (atmospheric forcing is not yet available from CESM2). The atmospheric forcing from CESM used here reflects influences from prescribed changes in solar irradiance, greenhouse gases (CO_2, CH_4, N_2O, O_3, CFCs), natural and anthropogenic aerosol burden, and interactions with and feedbacks from the biogeochemical components of CLM including aerosol (black carbon and dust) and nitrogen deposition, land cover change including harvest of wood, and prognostic leaf and stem area and canopy height determined by the carbon-nitrogen (CN) component of CLM. Here, the focus is on the urban simulation and CLM is run without biogeochemistry active (an exception being aerosol deposition which is required by the rural snow parameterization).

A control simulation (CON) is run in which the CLM4 version of the urban model (section 2) is coupled to CLM4. Three additional simulations with CLM5 are run to examine the effects of the new BEM and urban properties dataset; 1) the old version of the urban properties dataset (V1) and the old BEM (CLM5_UPV1_BEMV1), 2) V1 of the urban properties dataset and the new BEM (CLM5_UPV1_BEMV2), and 3) the new urban properties dataset (V2) and the new BEM (CLM5_UPV2_BEMV2).

Although both CLM5_UPV1_BEMV1 and the control simulation use version 1 of the urban properties dataset, the dataset is implemented differently in the two simulations. The control uses a single urban density class per grid cell selected from TBD, HD, and MD based on largest area, while the CLM5_UPV1_BEMV1 allows up to three density classes in each gridcell. Thus, comparison of CLM5_UPV1_BEMV1 to CON isolates the effects of implementing the three density classes plus any effects from the change in the parent CLM model (e.g., pervious canyon floor hydrology). Comparison of CLM5_UPV1_BEMV2 to CLM5_UPV1_BEMV1 isolates the effects of the new BEM. Comparison of CLM5_UPV2_BEMV2 to CLM5_UPV1_BEMV2 isolates the effects of the new urban properties dataset. Finally, comparison of CLM5_UPV2_BEMV2 to the CON simulation summarizes the effects of all changes since CLM4. The CON simulation is initialized from a CCSM4 preindustrial (1850) control simulation, while the CLM5 simulations are initialized from an 1850 offline CLM5 spinup simulation described in Lawrence et al. (2019).

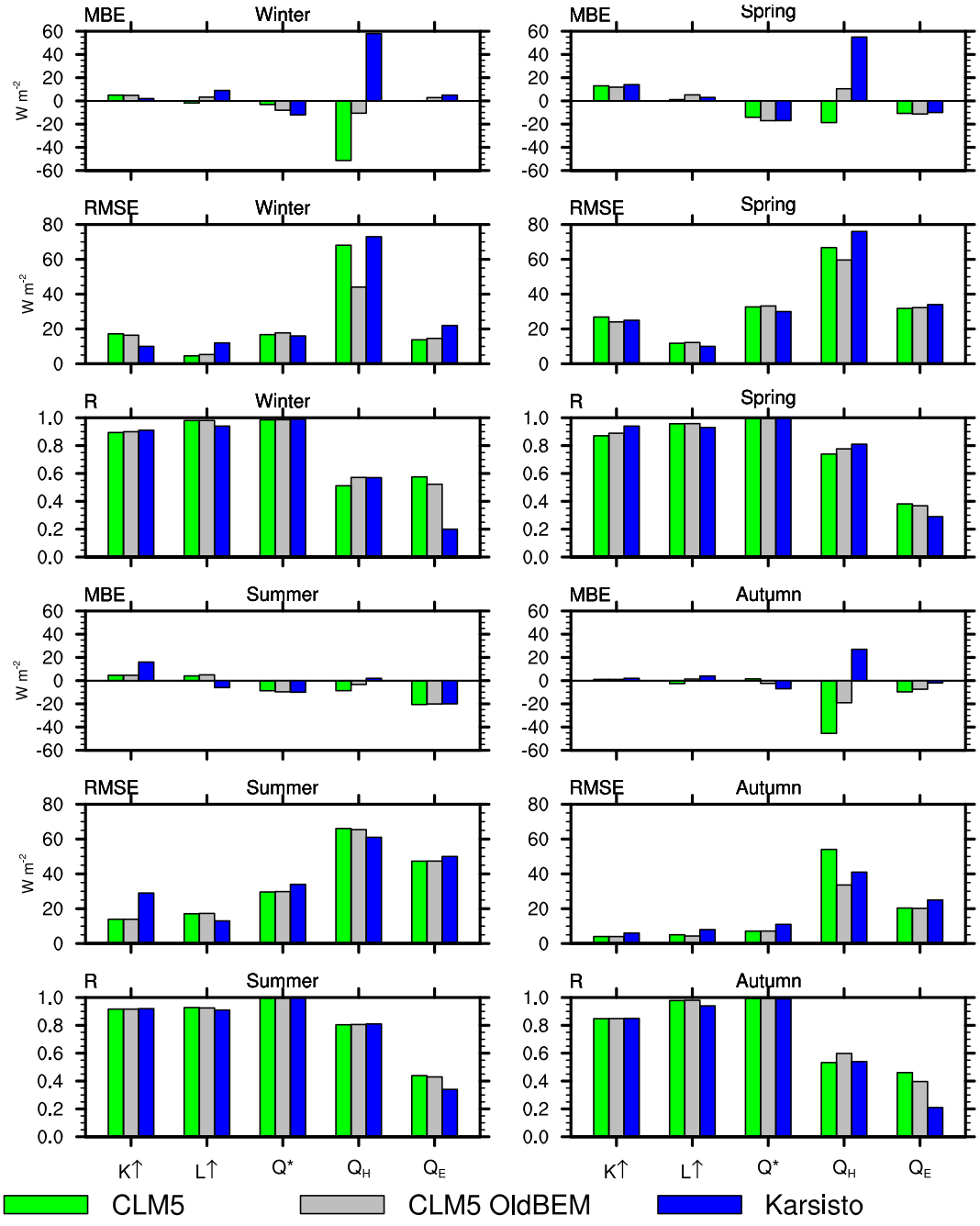

Figure 7. Summary statistics of hourly simulated (CLM5 in green, CLM5 with old BEM in grey) compared to observed reflected solar radiation ($K\uparrow$), emitted longwave radiation ($L\uparrow$), net radiation (Q^*), sensible heat (Q_H), and latent heat (Q_E) fluxes for the Hotel Torni site for four seasons in 2012 (Karsisto et al., 2015). Winter is 9 January – 14 March and 2 December – 31 December, Spring is 15 March – 14 May, Summer is 15 May – 6 October, and Autumn is 1 January – 8 January and 7 October – 1 December. Values denoted in blue are from the CLMU simulation reported in Karsisto et al. (2015). R is the Pearson correlation coefficient and the other statistics are described in Figure 5.

A primary focus of our previous research with CLMU has been the urban heat island (e.g., Oleson, 2012). Here, the focus is on urban temperature to avoid a lengthy discussion of changes in rural temperature caused by the many new vegetated-related processes in CLM5 (Lawrence et al., 2019). The global analysis examines the effects of the urban properties dataset and the building energy model on anthropogenic heat flux and urban near surface air temperature for 1986-2005.

Table 7
Summary statistics (MBE and RMSE) of half-hourly simulated compared to observed sensible heat (Q_H) and anthropogenic heat (Q_F) fluxes (W m^{-2}) and exterior surface temperatures of roof (T_{roof}), wall (T_{wall}), and road (T_{road}) (K) for sensitivity simulations described in section 7.2 for winter (15 January – 15 February 2005) at Tou04. The control (CON) simulation uses the default BEM parameters described in section 7.1.

	Q_H		Q_F		T_{roof}		T_{wall}		T_{road}	
	MBE	RMSE	MBE	RMSE	MBE	RMSE	MBE	RMSE	MBE	RMSE
CON	-19	34	-15	17	1.6	2.5	0.1	0.4	-0.2	1.0
ACH00	-18	34	-20	21	1.6	2.5	0.1	0.4	-0.2	1.0
ACH05	-19	34	-13	15	1.6	2.5	0.1	0.4	-0.2	1.0
E80	-18	34	-15	17	1.6	2.5	0.1	0.4	-0.2	1.0
E96	-18	34	-15	17	1.6	2.5	0.1	0.4	-0.2	1.0
FT03	-18	34	-15	17	1.6	2.5	0.1	0.4	-0.2	1.0
S2010	-10	29	-5	11	1.9	2.7	0.4	0.6	0.1	1.0

8. Results

8.1. Flux tower simulations

As expected, the results shown in Table 4 for Me93 and Table 5 for Vl92 indicate relatively small changes due to CLMU5 for these sites. However, there are improvements in MBE of 4-6 W m^{-2} and RMSE of 2-9 W m^{-2} for sensible heat (Q_H) depending on the site. The latent heat (Q_E) statistics are unchanged for Me93 and there is a small improvement in R^2 of 0.06 at Vl92 where the pervious canyon fraction is larger. As noted by Oleson, Bonan, Feddema, Vertenstein, and Grimmond (2008) the model performs significantly worse for Vl92 than Me93, however, the RMSE for all Vl92 fluxes are still lower than the mean RMSE for the urban models evaluated in Grimmond et al. (2010).

Results for the four seasons for Pres04 are shown in Figure 5. Only very small changes in the radiative fluxes are evident with MBE changing by at most 5 W m^{-2}, RMSE by 2 W m^{-2} and R^2 by 0.02. The largest changes are for the MBE in outgoing longwave which increases by 5 W m^{-2} in spring and decreases by 3 W m^{-2} in summer, due to warmer surface temperatures in spring and cooler temperatures in summer (not shown). In general, Q_H is higher in the new model in winter and spring which improves the MBE by 8 and 4 W m^{-2}, respectively, and lower in summer which improves MBE by 15 W m^{-2}. Q_H RMSE is similar in winter and spring and slightly improved in summer. Conversely, Q_E is lower in winter and spring which degrades MBE by 5 W m^{-2}, but higher in summer which improves MBE by 16 W m^{-2}. The notable improvement in the summer MBE for Q_H and Q_E is likely due to less soil moisture stress for the pervious canyon floor in CLM5 (not shown). The hydrologically active soil column in CLM5 is now 8.5 m in depth as opposed to about 3.5 m in CLM4. A uniform rooting profile is specified for the pervious canyon floor which means that more water is accessible and the bulk parameterization for evaporation (section 2) is more resilient to drying. The storage heat flux improves slightly in all seasons for MBE and RMSE but degrades for R^2. For the entire period of simulation, the performance of CLMU5 is still comparable to the version reported in Grimmond et al. (2011) (model 43).

Figure 6 and Table 6 compare results from CLMU5 to the simulation reported in Demuzere et al. (2013) for Tou04. For this site, the new BEM is the cause of the largest differences, particularly in winter where the anthropogenic heat flux (Q_F) and Q_H decrease, the roof and wall surface temperatures (T_{roof} and T_{wall}) and canyon air temperature (T_{canyon}) decrease, and the road temperature (T_{road}) increases. Outgoing longwave radiation ($L\uparrow$) is lower in response to the lower surface temperatures. Generally, the changes in winter are for the better with respect to observations, particularly for Q_F with lower MBE and RMSE and a doubling of R^2, and for $L\uparrow$, T_{roof}, and T_{wall} with lower MBE and RMSE. Although Q_H is reduced the absolute value of the MBE is about the same and no improvements are noted for RMSE and R^2. The small increase in T_{road} is due to the wasteheat added to the canyon floor which was not accounted for in Demuzere et al. (2013).

Similar behaviour of Q_F and Q_H is seen for the transition seasons of spring and fall, however, the changes with respect to the observations are more mixed. The decrease in Q_F leads to a larger negative MBE in both seasons but improvements in RMSE and R^2. The MBE and RMSE for Q_H are improved in spring but about the same in fall. The MBE and RMSE for T_{roof} and T_{wall} are improved in the fall. In summer, the Q_H MBE is

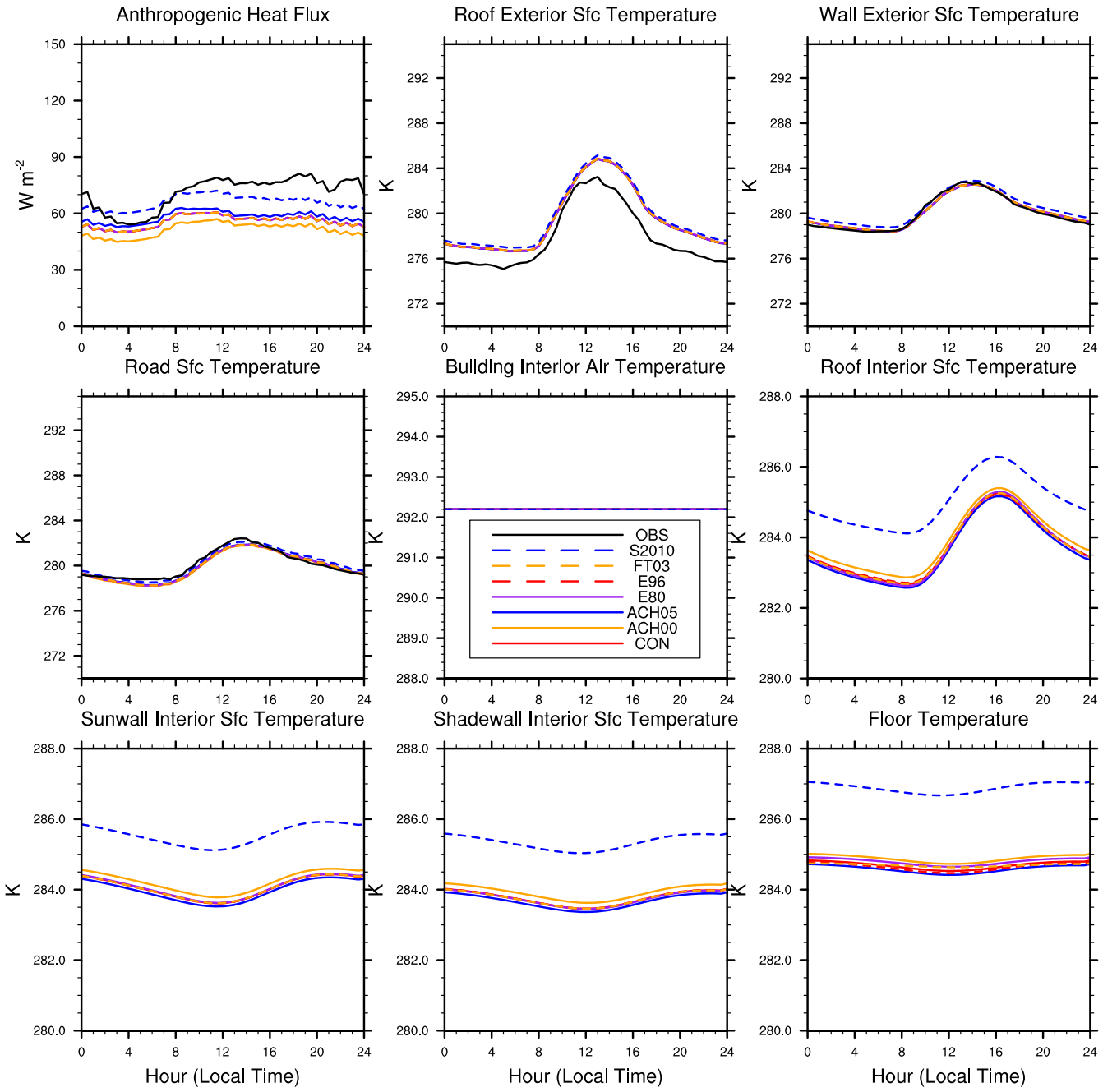

Figure 8. Average diurnal cycles of anthropogenic heat flux, roof and wall exterior and interior surface temperatures, road surface temperature, building interior air temperature, and floor temperature (K) for sensitivity simulations described in section 7.2 for winter (15 January – 15 February 2005) at Tou04. The control (CON) simulation uses the default BEM parameters described in section 7.1.

improved by 13 W m^{-2} due to higher Q_E while Q_F is unchanged. Overall, the BEM produces lower Q_F than observed in all seasons. However, this is expected because the observed anthropogenic heat flux for Tou04 results from space heating and all other domestic uses (Pigeon et al., 2007) while the model accounts for space heating only.

Figure 7 compares results from CLMU5 with and without the new BEM to the simulation reported in Karsisto et al. (2015) for the Hotel Torni site. The large positive bias in Q_H in winter, spring, and autumn in the Karsisto et al. (2015) simulation is greatly reduced when the new urban properties data are used

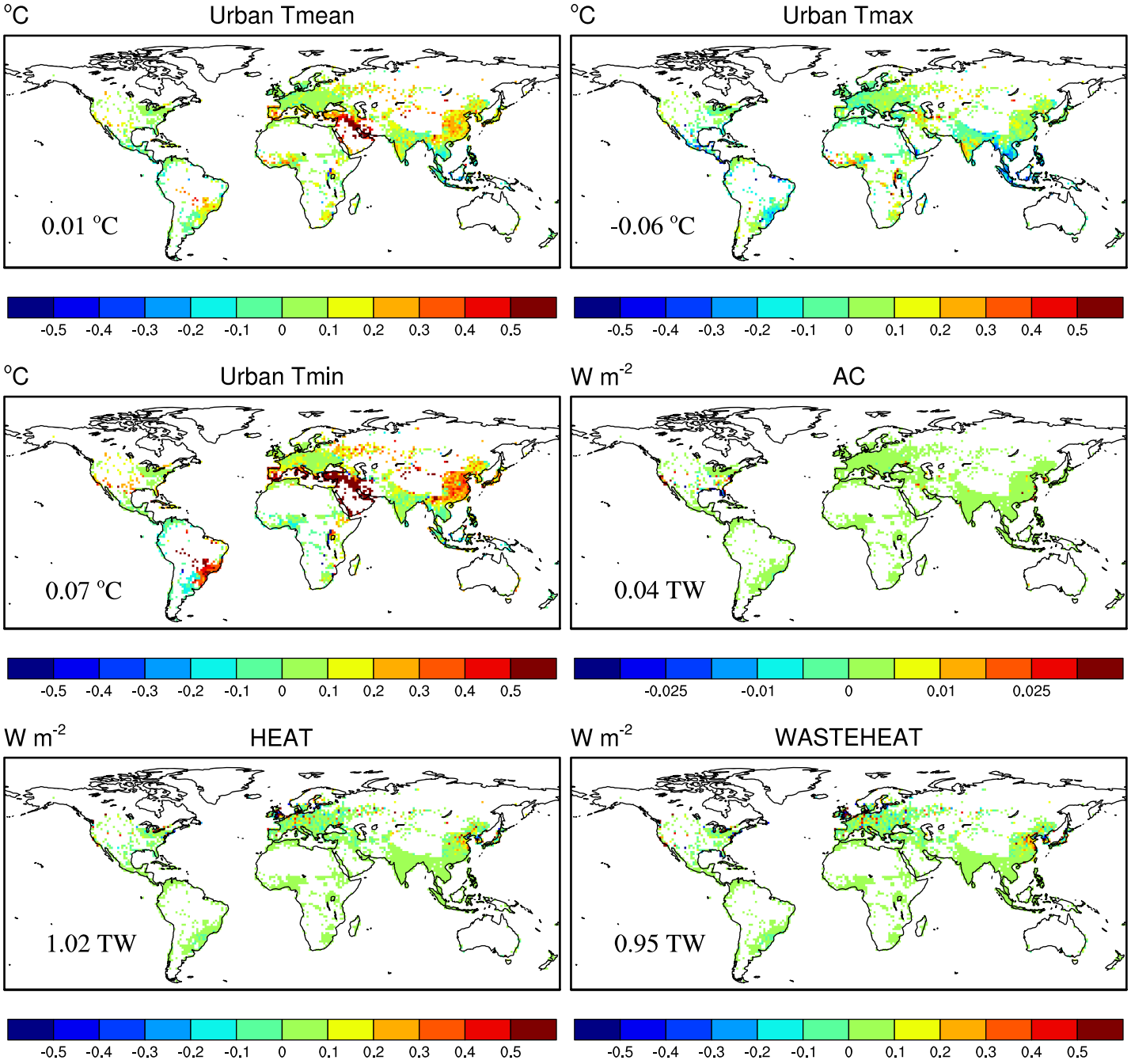

Figure 9. Differences in urban annual mean, daily maximum and minimum temperature, air conditioning (AC), space heating (HEAT), and wasteheat between the CLM5_UPV1_BEMV1 and CON simulations for 1986-2005. Numbers in the lower left corner of the plots for Tmean, Tmax, and Tmin represent the global mean difference (°C) and the numbers for AC, HEAT, and WASTEHEAT represent the global total difference (TW).

(CLM5 OldBEM in Figure 7). This is a direct result of prescribing increased insulation in the walls and roof thereby reducing space heating and sensible heat. In particular, the Q_H MBE is reduced from 58 W m^{-2} to -11 W m^{-2} in winter and RMSE is reduced from 73 to 44 W m^{-2}. On the other hand, adding the new BEM further reduces space heating and sensible heat such that the MBE increases from -11 to -51 W m^{-2} and RMSE increases from 44 to 68 W m^{-2} in winter (CLM5 in Figure 7). The old BEM held the interior temperatures of the walls and roof right at the heating setpoint, while the new BEM operates on the interior building air temperature and the walls and roof interior temperatures are thus allowed to be colder which reduces

Table 8
Global urban air conditioning [AC; Eq. (10)], space heating [HEAT; Eq. (11)], wasteheat [WSTH; Eq. (13)], building heat (BUILD; the net sink of energy for the climate system in BEMV1 described in section 4), and total anthropogenic heat flux (AHF) (all in terrawatts) for the simulations described in section 7.3. The AHF is calculated as HEAT plus WSTH in all cases, except that numbers for AHF in parentheses for the CON and CLM5_UPV1_BEMV1 simulations are calculated from BUILD plus AC plus WSTH and represents the total energy into the climate system (Oleson, 2012).

	AC	HEAT	WSTH	BUILD	AHF
			2005		
CON	0.13	4.41	5.88	-1.01	10.29 (5.00)
CLM5_UPV1_BEMV1	0.18	5.34	6.80	1.71	12.14 (8.69)
CLM5_UPV1_BEMV2	0.05	2.65	0.56	0.00	3.21
CLM5_UPV2_BEMV2	0.04	2.59	0.54	0.00	3.13
			1986-2005		
CON	0.11	4.91	6.43	-0.60	11.34 (5.94)
CLM5_UPV1_BEMV1	0.14	5.93	7.38	2.01	13.31 (9.53)
CLM5_UPV1_BEMV2	0.04	2.94	0.61	0.00	3.55
CLM5_UPV2_BEMV2	0.03	2.88	0.59	0.00	3.47

the amount of space heating required. This implies that the generic wall and roof thermal properties from the urban properties dataset are still not entirely appropriate for this specific location (the model properties represent all of northern Europe, while being compared to specific buildings in Helsinki, Finland). Similar behaviour is seen in spring and autumn, while the behaviour of the model in summer (with no air conditioning) is essentially unchanged.

In summary, CLMU5 performance for Me93 and Vl92 essentially remains the same as the previous model version because heating and air conditioning is not active and the pervious canyon floor fraction is small. The performance for Pres04 is also similar to the previous model version except that there is some reduction in model error in sensible and latent heat in summer due to less soil moisture stress for the pervious canyon floor. The new BEM results in a modest reduction in model error of anthropogenic heat flux and surface and air temperatures for Tou04 in winter. Results are more mixed for transition seasons of spring and fall. For the Hotel Torni site, model error in sensible heat in winter, spring, and autumn is greatly reduced due to the increased insulation in walls and roof in the new urban properties dataset. However, addition of the new BEM further reduces space heating and thus sensible heat such that the net effect of the properties data and BEM results in only a small improvement in sensible heat in winter and autumn, although a larger improvement in spring.

8.2. Sensitivity simulations

The sensitivity of the model to the BEM input parameters for the Tou04 site is largest in winter and is summarized in Table 7 for MBE and RMSE and Figure 8 which shows the average diurnal cycle for anthropogenic heat flux and interior and exterior surface temperatures. The model is fairly insensitive to emissivity changes and floor thickness with respect to the model fluxes and temperatures shown in Figure 8 (E80, E96, FT03). In summer, the thicker floor (FT03) results in a slight dampening of the amplitude of the diurnal cycle of floor temperature (not shown). Eliminating air infiltration (ACH00) results in a small reduction in Q_F while increasing the infiltration of outside air (ACH05) increases Q_F. These degrade and improve the simulation of Q_F in term of MBE, respectively. Surface temperatures and Q_H are relatively insensitive to these changes.

The model is most sensitive to the change in the interior heat transfer coefficients (S2010). The MBE of both Q_H and Q_F are improved by 9-10 W m^{-2} with some reduction in the RMSE as well in the S2010 simulation. The interior surface temperatures of roof, walls, and floor are much warmer (1.5-2.0 K) as heat is transferred more readily from the building interior to the interior surfaces (Figure 8). This results in more heat being transferred to the outside of the building resulting in an increase in MBE of exterior T_{roof} and T_{wall} of about 0.3 K (Table 7).

8.3. Global simulations

First, we examine the effects of including the multiple density classes instead of the dominant density class by area on AHF and urban temperature. The spatial patterns of differences in urban mean, daily maximum (Tmax) and minimum temperature (Tmin) and AHF components for CLM5_UPV1_BEMV1 compared to the control are shown in Figure 9, with a summary of global average AHF components in Table 8.

Global AHF increases from about 10.3 TW to 12.1 TW for year 2005 due to increases in AC, heating, and wasteheat (Table 8). Global average urban mean temperature is essentially unchanged, although regions such as the Arabian Peninsula and eastern China for example are warmer and Indonesia is cooler (Figure 9). Generally, any changes in Tmax are smaller than Tmin, with Tmax cooler and Tmin warmer. These changes are consistent with the addition of fractions of the high density (HD) and tall building district (TBD) urban density classes in CLM5_UPV1_BEMV1. The higher density classes have larger canyon height-to-width ratios resulting in more storage of heat during the day (cooler Tmax) and the release of that heat at night (warmer Tmin) (see Oleson et al. (2015) in which separate simulations over the U.S. were conducted for

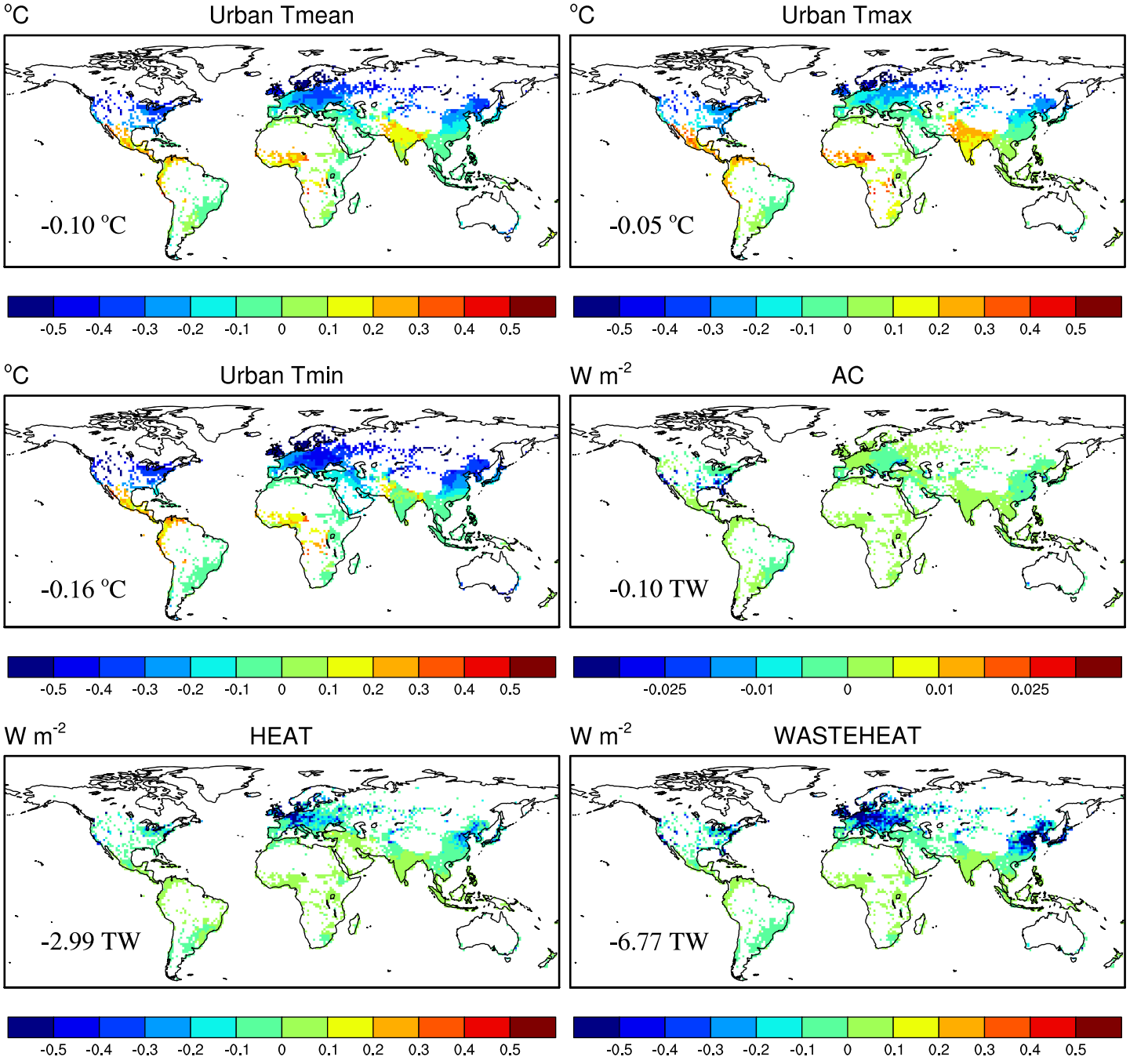

Figure 10. As in Figure 9 but for differences between CLM5_UPV1_BEMV2 and CLM5_UPV1_BEMV1.

each of the three density classes). Some of the decrease in Tmax is likely offset by a decrease in pervious canyon floor for these density classes that lowers evaporation and increases daytime temperature. Generally, more space heating at high latitudes is required (for example in Europe and Northern China) due to the larger building volumes of these density classes, depending on their presence and fraction within a grid cell. Other properties such as wall/roof thermal properties may play a role as well. The advantage of the multiple density classes is that only a single simulation needs to be run to explore the effects of different density classes on urban climate. Averaged results are shown in Figure 9 but additional model output for each density class can be requested from the model.

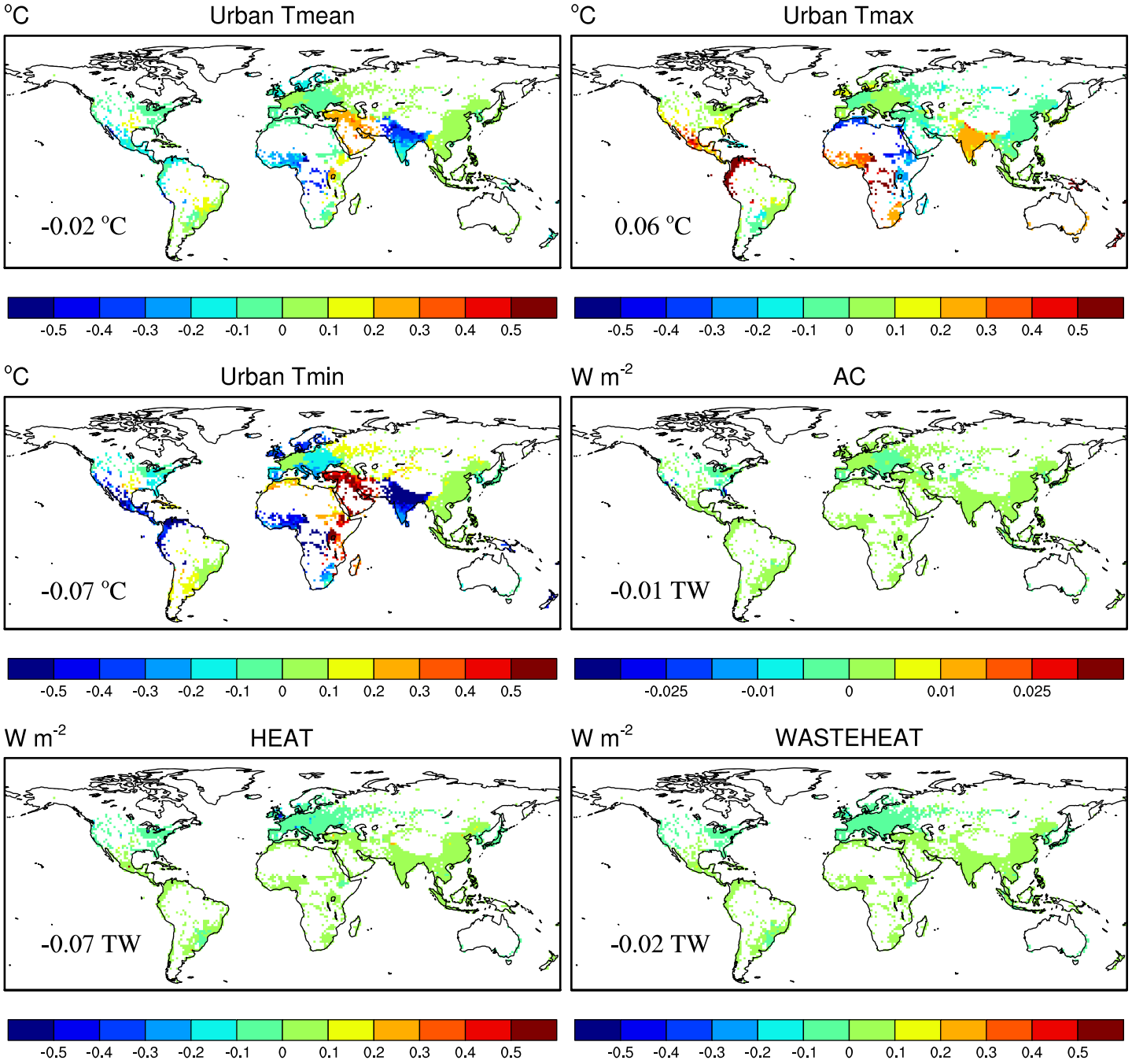

Figure 11. As in Figure 9 but for differences between CLM5_UPV2_BEMV2 and CLM5_UPV1_BEMV2.

Next, the effects of the new BEM alone are shown in Figure 10 and Table 8 (CLM5-UPV1_BEMV2 compared to CLM5_UPV1_BEMV1). A dominant feature in Figure 10 is the reduction in space heating and wasteheat at high latitudes in winter where space heating is required. Urban air temperature is lower in response to this because there is less wasteheat in the form of sensible heat transferred into the urban canyon. The reduction in the AHF fluxes can be attributed in part to the fact that the old BEM held the interior temperatures of the walls and roof right at the building temperature setpoint (Oleson, Bonan, et al., 2010) while the new BEM operates on the interior building air temperature and thus the interior wall and roof temperatures are

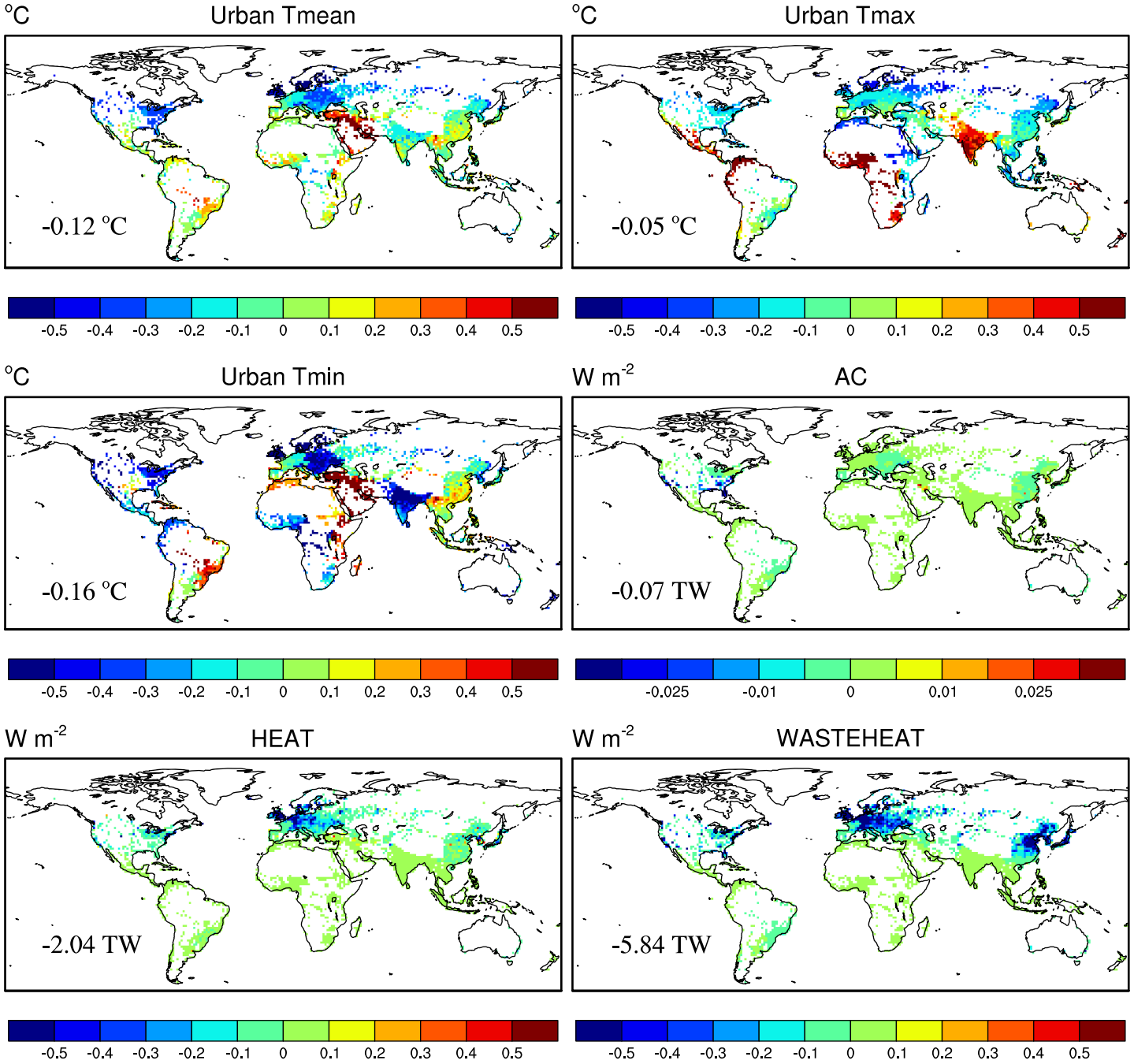

Figure 12. As in Figure 9 but for differences between CLM5_UPV2_BEMV2 and CON.

allowed to be colder in the case of heating (and warmer in the case of AC). The wasteheat factors are also lower in the new BEM (section 4). In contrast, the new BEM produces warmer air temperatures in most tropical regions such as Central America, Central Africa, the Sahel, and India, despite little to no change in AHF fluxes. As noted in section 4, the old BEM created a net sink of energy in these regions. The higher temperatures in the new BEM are a result of energy being conserved. Air conditioning is reduced in summer in the southern U.S., southern Europe, and China, resulting in a global annual reduction in AC of 0.1 TW. The net result is that the total global AHF is reduced by almost a factor of four from 12.1 TW to 3.2 TW for

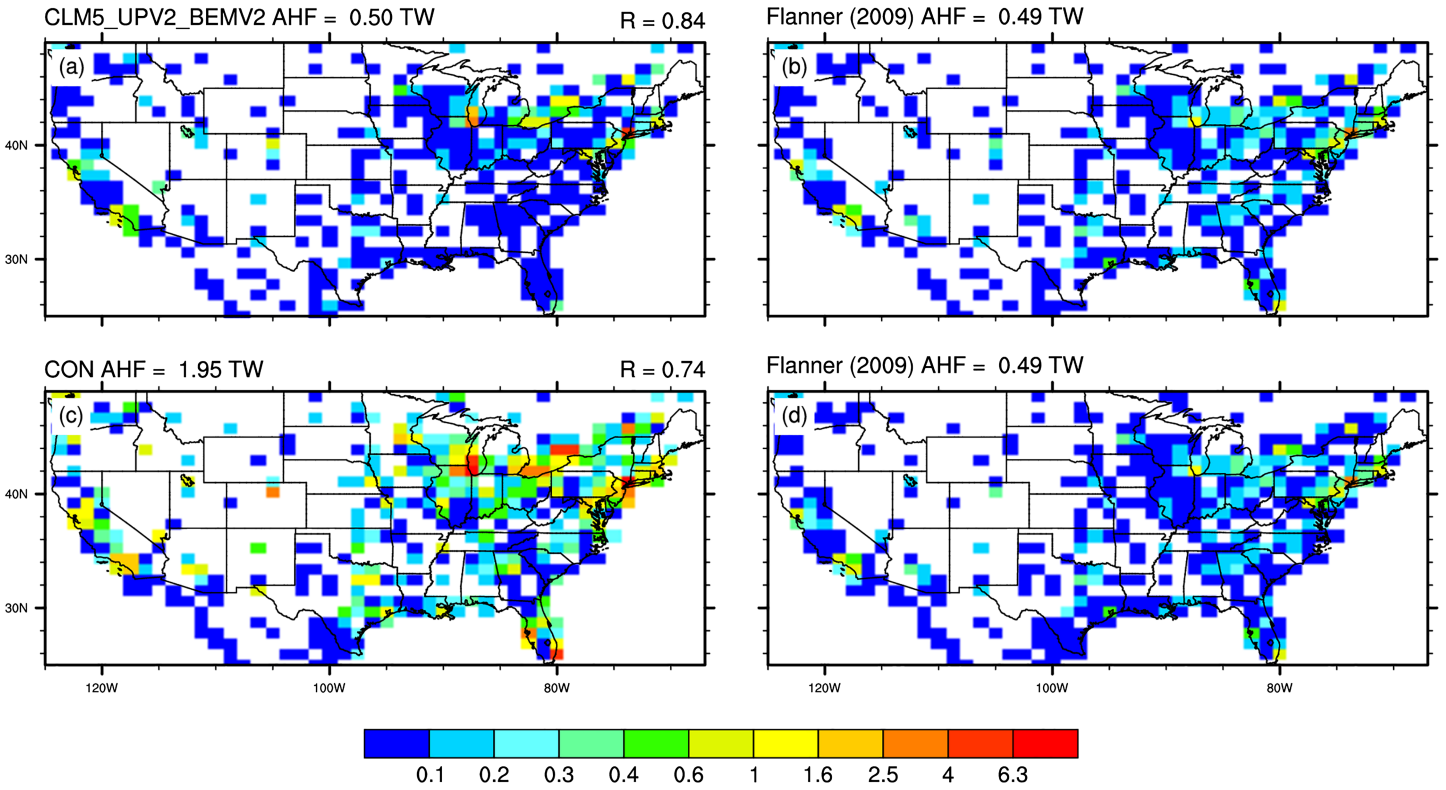

Figure 13. Comparison of anthropogenic heat flux due to space heating and air conditioning (AHF) over the U.S. from the (a) CLM5_UPV2_BEMV2 and (c) CON simulations, and (b) and (d) Flanner (2009) dataset (W m^{-2}). The Flanner (2009) total AHF from all sources has been multiplied by 16% to adjust it for energy due only to space heating and air conditioning (section 4). The model and the Flanner (2009) data have been masked for each other's urban areas. R is the pattern correlation between the model simulations and Flanner (2009) Figure 14.

year 2005 which compares well with the observational estimate of 3.1 TW derived in section 4. The 1986-2005 climatology for AHF is somewhat higher at 3.5 TW.

The effects of the V2 urban properties data (CLM5_UPV2_BEMV2 compared to CLM5_UPV1_BEMV2) are shown in Table 8 for AHF and Figure 11 for urban temperature and AHF components. There is a small decrease in AHF of about 0.08 TW for year 2005 and the 1986-2005 climatology. The decrease occurs at higher latitudes, particularly in Europe and the northern U.S. Figure 11 shows the spatial patterns of differences in urban temperature in each of the thirty-three regions of urban data, and the impact of using a single building type compared to a combination of multiple building types to represent each of the three urban classes. In general, changes in Tmax and Tmin are opposite in sign. For example, Tmax is warmer in India while Tmin is cooler, mostly due to higher roof R-values which results in less storage of heat during the day (warmer Tmax) and less release of heat at night (cooler Tmin). Similar behaviour is seen in northwestern South America, the Sahel, and Central America. In some regions, the Arabian Peninsula for example, the change in urban temperature is opposite (cooler Tmax, warmer Tmin), likely due to lower wall R-values and albedo for the MD class (not shown).

Figure 12 summarizes the combined effects of the parent CLM model, the addition of the TBD and HD density classes, and the new BEM and urban properties data. The main feature of the new model is a broad reduction in urban temperature and AHF at higher latitudes that is due to the new BEM (Figure 10) and to a lesser extent the new urban properties data (Figure 11). Spatial variability in the differences at other latitudes is caused primarily by the combined effects of the addition of TBD and HD classes (Figure 9) and the new urban properties (Figure 11). Figure 13 (U.S.) and Figure 14 (Europe) indicate that AHF for the new model (CLM5_UPV2_BEMV2) compares well with the Flanner (2009) estimate on a regional basis as well as globally. The pattern correlation between the new BEM and Flanner (2009) is higher in both regions compared to the control and the total AHF over each region is significantly improved.

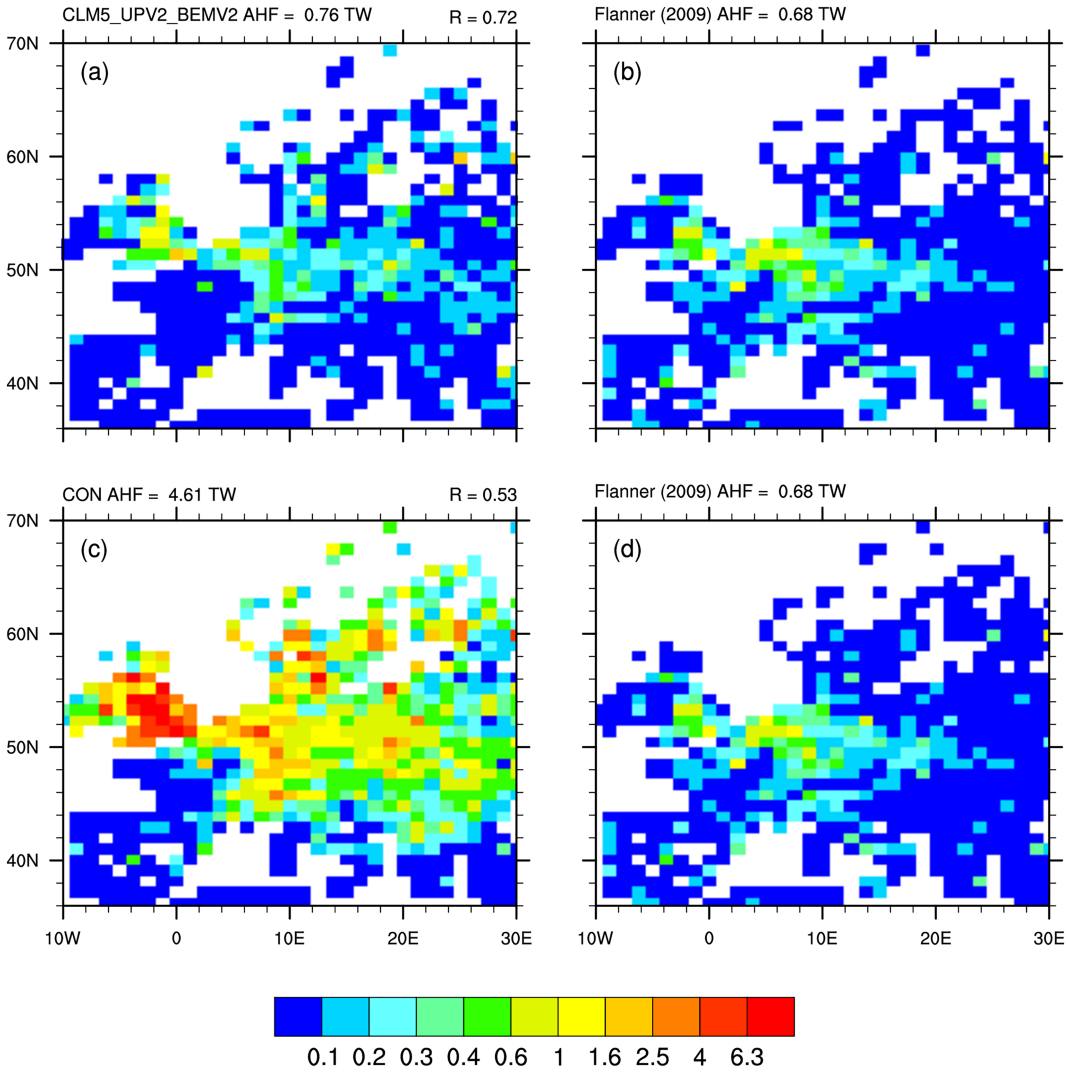

Figure 14. As in Figure 13 but for Europe. The Flanner (2009) total AHF from all sources has been multiplied by 25% to adjust it for energy due only to space heating and air conditioning (section 4).

9. Conclusions

The CLMU was created to simulate urban climates within the CESM modeling framework to evaluate the combined impacts of global scale climate change and local urban climates on the majority of the world's human population. To function in this global context, the model has to operate under all climate conditions and represent urban characteristics reasonably well across the globe. However, lack of information on urban systems in many parts of the world require significant generalization of urban morphology and urban fabric characteristics. Some of these short-comings have become apparent since the initial version of the model, and in this paper we outline improvements to the model in terms of the number of urban classes that can be simulated within a grid cell, the inclusion of a more realistic BEM, corrections and improvements to the model input parameters, and a structure for better simulating the interactions between the urban fabric and the climate system. By changing the way wall and roof facets are built and processed, there is a significant improvement in how energy exchanges are simulated with a better representation of the parallel energy fluxes through walls and window facets. In addition, we have developed a tool set to facilitate the construction of more detailed urban fabrics (wall and roof structures) and an improved capability to develop scenarios for inclusion in IPCC and other assessment studies.

Specific outcomes of the updated model show that the new BEM greatly improves estimates of energy consumption associated with heating and air conditioning usage on a global scale, with simulated energy usage very close to those estimated from observations [3.2 TW vs 3.1 TW from Flanner, 2009]; this is a threefold improvement from the overestimate in the previous model version. Overall, the addition of the BEM and a few corrections to wall and roof properties in the original J2010 dataset have led to slight improvements in the simulation of observational measurements at various flux tower sites. Differences from observations relate to model design (the canyon model is a significant simplification of the complexity of the observation sites), model error (specifically with our ability to replicate the turbulent fluxes (Q_H and Q_E)), but are also partly due to differences between the model input data representing building generalized regional scale building characteristics versus actual building characteristics at the study sites (e.g. Helsinki).

Overall improvements are relatively slight in the context of how well CLMU simulates urban climates at specific sites, this improvement comes relative to the previous version of CLMU that placed in the upper third of the 32 urban model intercomparison project (Grimmond et al., 2011). Given the relatively simplicity and computational efficiency of the model, the limited set of input parameters required (by necessity given its global application with data scarce regions), and the broad set of climates where it is applied these results are promising and make the model effective for simulating urban climate impacts within the CESM framework. The addition of the new BEM helps to improve the climate simulations and also provides a major improvement in our ability to simulate energy usage and emissions associated with urban HAC. With these improvements, the model will greatly facilitate its use for climate impact assessment studies under various climate and urban development scenarios in the CESM.

A couple of potential model development pathways are being considered for the next version of the model. First, the generally poorer results for the model for latent flux in the tower site comparisons, consistent with the findings of the international urban energy balance models comparison project (Grimmond et al., 2010, 2011), indicate a need to develop a more sophisticated parameterization of evapotranspiration in urban areas, perhaps in a manner similar to recent work by Lee and Park (2008), Lemonsu et al. (2012), and Li et al. (2016) in which vegetation is modelled explicitly instead of the bulk parameterization currently used in CLMU. Second, as demonstrated by Stewart et al. (2014), it would likely be beneficial to transition from the current urban density class representation in the model to the Local Climate Zone (LCZ) classification system (Stewart & Oke, 2012). Such a transition would leverage the large amount of work being done to develop and characterize comprehensive datasets on urban areas (e.g., the World Urban Database and Access Portal Tools [WUDAPT], Bechtel et al., 2015; Ching et al., 2018) as well as facilitate comparisons with the growing number of urban models that have adopted this classification system (e.g., Brousse et al., 2016) and improve validation efforts.

Model and tools availability

The CLMU5 code is publicly available as part of the CLM5.0 release through the Community Terrestrial System Model (CTSM) git repository (https://github.com/ESCOMP/ctsm). The THESIS urban properties tool is available at http://www.cesm.ucar.edu/projects/thesis/thesis-urbanproperties-tool.html.

Data AvailabilityStatement

The simulation data is archived and publicly available at the UCAR/NCAR Climate Data Gateway, https://doi.org/10.5065/d6154fwh. The 0.05deg V2 urban dataset is available from the CESM input data repository (https://svn-ccsm-inputdata.cgd.ucar.edu/trunk/inputdata/) as an optional surface data input for CLM5.

Acknowledgments
The CESM project is supported primarily by the National Science Foundation (NSF). This material is based upon work supported by the NSF under Grant Number AGS-1243095 and upon work supported by the National Center for Atmospheric Research (NCAR), which is a major facility sponsored by the NSF under Cooperative Agreement No. 1852977. K.W. Oleson was supported in part by NASA grant NNX10AK79G (the SIMMER project) and the NCAR Weather and Climate Impacts Assessment Science Program (WCIASP). We would like to acknowledge the efforts of Brian Kauffman (NCAR) in developing the THESIS urban properties tool. Computing and data storage resources, including the Cheyenne supercomputer (doi:10.5065/D6RX99HX), were provided by the Computational and Information Systems Laboratory (CISL) at NCAR. We thank all the scientists, software engineers, and administrators who contributed to the development of CESM2. We gratefully acknowledge two anonymous reviewers for constructive comments that substantially improved the manuscript.

References

Bechtel, B., Alexander, P., Bohner, J., Ching, J., Conrad, O., Feddema, J., et al. (2015). Mapping local climate zones for a worldwide database of the form and function of cities. *ISPRS International Journal of Geo-Information*, *4*, 199–219. https://doi.org/10.3390/ijgi4010199

Brousse, O., Martilli, A., Foley, M., Mills, G., & Bechtel, B. (2016). WUDAPT, an efficient land use producing data tool for mesoscale models? Integration of urban LCZ in WRF over Madrid. *Urban Climate*, *17*, 116–134. https://doi.org/10.1016/j.uclim.2016.04.001

Bueno, B., Pigeon, G., Norford, L. K., Zibouche, K., & Marchadier, C. (2012). Development and evaluation of a building energy model integrated in the TEB scheme. *Geoscientific Model Development*, *5*, 433–448. https://doi.org/10.5194/gmd-5-433-2012

Buzan, J., Oleson, K., & Huber, M. (2015). Implementation and comparison of a suite of heat stress metrics within the Community Land Model version 4.5. *Geoscientific Model Development*, *8*, 151–170. https://doi.org/10.5194/gmd-8-151-2015

CDC (Centers for Disease Control) (2006). Heat-related Deaths – United States, 1999-2003, Mortality and Morbidity Weekly Report published by the Centers for Disease Control, July 28, 2006/55(29):796-798, http://www.cdc.gov/mmwr/preview/mmwrhtml/mm5529a2.htm

Ching, J., Mills, G., Bechtel, B., See, L., Feddema, J., Wang, X., et al. (2018). World Urban Database and Access Portal Tools (WUDAPT), an urban weather, climate and environmental modeling infrastructure for the Anthropocene. *Bulletin of the American Meteorological Society*, *99*(9), 1907–1924. https://doi.org/10.1175/BAMS-D-16-0236.1

Coutts, A. M., Beringer, J., & Tapper, N. J. (2007a). Characteristics influencing the variability of urban CO2 fluxes in Melbourne, Australia. *Atmospheric Environment*, *41*, 51–62. https://doi.org/10.1016/j.atmosenv.2006.08.030

Coutts, A. M., Beringer, J., & Tapper, N. J. (2007b). Impact of increasing urban density on local climate: Spatial and temporal variations in the surface energy balance in Melbourne, Australia. *Journal of Applied Meteorology and Climatology*, *46*, 477–493. https://doi.org/10.1175/jam2462.1

Demuzere, M., Oleson, K., Coutts, A. M., Pigeon, G., & van Lipzig, N. P. M. (2013). Simulating the surface energy balance over two contrasting urban environments using the Community Land Model Urban. *International Journal of Climatology*, *33*, 3182–3205. https://doi.org/10.1002/joc.3656

Energy Information Administration (EIA) (2009). 2005 residential energy consumption survey, energy consumption and expenditures Table US11, available at: http://www.eia.doe.gov/emeu/consumption/index.html.

Energy Information Administration (EIA) (2008). 2003 commercial buildings energy consumption survey, energy end-use consumption Table E1A, available at: http://www.eia.doe.gov/emeu/consumption/index.html.

Energy Information Administration (EIA) (2012). Energy consumption estimates by sector, 1949-2012, available at: http://www.eia.gov/totalenergy/data/annual/index.cfm#consumption.

EnergyPlus (2012). EnergyPlus Engineering Reference, U.S. Department of Energy, available at: http://apps1.eere.energy.gov/buildings/energyplus/pdfs/engineeringreference.pdf.

Engineering Toolbox (2014). Emissivity coefficients of some common materials, available at: http://www.engineeringtoolbox.com/emissivity-coefficients-d_447.html.

European Technology Platform on Renewable Heating and Cooling (2011). 2020–2030–2050 Common Vision for the Renewable Heating & Cooling sector in Europe, available at: www.rhc-platform.org.

Feddema, J., Kauffman, B. (2016). "Urban Properties Tool (Version 1.2)." NCAR THESIS Tools Library. Retrieved from: https://svn-iam-thesis-release.cgd.ucar.edu/urban_properties/. DOI: https://doi.org/10.5065/D6R78CMT.

Flanner, M. G. (2009). Integrating anthropogenic heat flux with global climate models. *Geophysical Research Letters*, *36*, L02801. https://doi.org/10.1029/2008gl036465

Gent, P. R., Danabasoglu, G., Donner, L. J., Holland, M. M., Hunke, E. C., Jayne, S. R., et al. (2011). The Community Climate System Model Version 4. *Journal of Climate*, *24*, 4973–4991. https://doi.org/10.1175/2011jcli4083.1

Grimmond, C. S. B., & Oke, T. R. (2002). Turbulent heat fluxes in urban areas: Observations and a local-scale urban meteorological parameterization scheme (LUMPS). *Journal of Applied Meteorology*, *41*, 792–810. https://doi.org/10.1175/1520-0450(2002)041<0792:thfiua>2.0.co;2

Grimmond, C. S. B., Blackett, M., Best, M. J., Barlow, J., Baik, J. J., Belcher, S. E., et al. (2010). The International Urban Energy Balance Models Comparison Project: First Results from Phase 1. *Journal of Applied Meteorology and Climatology*, *49*, 1268–1292. https://doi.org/10.1175/2010jamc2354.1

Grimmond, C. S. B., Blackett, M., Best, M. J., Baik, J. J., Belcher, S. E., Beringer, J., et al. (2011). Initial results from phase 2 of the international urban energy balance model comparison. *International Journal of Climatology*, *31*(2), 244–272. https://doi.org/10.1002/joc.2227

Hadley, S. W., Erickson, D. J., Hernandez, J. L., Broniak, C. T., & Blasing, T. J. (2006). Responses of energy use to climate change: A climate modeling study. *Geophysical Research Letters*, *33*, L17703. https://doi.org/10.1029/2006gl026652

International Energy Agency (IEA) (2011). Technology Roadmap, Energy-efficient Buildings: Heating and Cooling Equipment, OECD/IEA, Paris, France, available at: http://www.iea.org.

International Energy Agency (IEA) (2013). Transition to Sustainable Buildings, Strategies and Opportunities to 2050, OECD/IEA, Paris, France, available at: http://www.iea.org/publications/.

Jackson, T. L., Feddema, J. J., Oleson, K. W., Bonan, G. B., & Bauer, J. T. (2010). Parameterization of Urban Characteristics for Global Climate Modeling. *Annals of the Association of American Geographers*, *100*, 848–865.

Karsisto, P., Fortelius, C., Demuzere, M., Grimmond, C. S. B., Oleson, K. W., Kouznetsov, R., et al. (2015). Seasonal surface urban energy balance and wintertime stability simulated using three land-surface models in the high-latitude city Helsinki. *Quarterly Journal of the Royal Meteorological Society A*, *142*(694), 401–417. https://doi.org/10.1002/qj.2659

Kikegawa, Y., Genchi, Y., Yoshikado, H., & Kondo, H. (2003). Development of a numerical simulation system toward comprehensive assessments of urban warming countermeasures including their impacts upon the urban buildings' energy-demands. *Applied Energy*, *76*, 449–466. https://doi.org/10.1016/s0306-2619(03)00009-6

Kraus, C., Hirmas, D., & Roberts, J. (2013). Microbially indurated rammed earth: A long awaited next phase of earthen architecture. In C. Jarrett, K. Kim, & N. Senske (Eds.), *The Visibility of Research, Proceedings of the 2013 Architectural Research Centers Consortium* (pp. 58–65). Charlotte, NC: University of North Carolina Charlotte.

Kraus, C., Hirmas, D., & Roberts, J. (2015). Compressive strength of blood stabilized earthen architecture. In C. Mileto, F. Vegas, L. García Soriano, & V. Christini (Eds.), *Earthen Architecture: Past, Present and Future* (pp. 217–220). London, UK: Taylor & Francis Group.

Lawrence, D. M., Oleson, K. W., Flanner, M. G., Thornton, P. E., Swenson, S. C., Lawrence, P. J., et al. (2011). Parameterization Improvements and Functional and Structural Advances in Version 4 of the Community Land Model. *Journal of Advances in Modeling Earth Systems*, *3*, M03001. https://doi.org/10.1029/2011ms000045

Lawrence, D. M., Fisher, R. A., Koven, C. D., Oleson, K. W., Swenson, S. C., Bonan, G., et al. (2019). The Community Land Model version 5: description of new features, benchmarking, and impact of forcing uncertainty. *Journal of Advances in Modeling Earth Systems*. https://doi.org/10.1029/2018MS001583

Lee, S. H., & Park, S. U. (2008). A vegetated urban canopy model for meteorological and environmental modelling. *Boundary-Layer Meteorology*, *126*, 3–102. https://doi.org/10.1007/s10546-007-9221-6

Lemonsu, A., Masson, V., Shashua-Bar, L., Erell, E., & Pearlmutter, D. (2012). Inclusion of vegetation in the Town Energy Balance model for modelling green areas. *Geoscientific Model Development*, *5*, 1377–1393. https://doi.org/10.5194/gmd-5-1377-2012

Li, D., Malyshev, S., & Shevliakova, E. (2016). Exploring historical and future urban climate in the Earth System Modeling framework: 1. Model development and evaluation. *Journal of Advances in Modeling Earth Systems*, *8*, 917–935. https://doi.org/10.1002/2015MS000578

Masson, V. (2000). A physically-based scheme for the urban energy budget in atmospheric models. *Boundary-Layer Meteorology*, *94*, 357–397. https://doi.org/10.1023/a:1002463829265

Masson, V., Gomes, L., Pigeon, G., Liousse, C., Pont, V., Lagouarde, J. P., et al. (2008). The Canopy and Aerosol Particles Interactions in TOulouse Urban Layer (CAPITOUL) experiment. *Meteorology and Atmospheric Physics*, *102*(3-4), 135–157. https://doi.org/10.1007/s00703-008-0289-4

Oke, T. R., Spronken-Smith, R. A., Jauregui, E., & Grimmond, C. S. B. (1999). The energy balance of central Mexico City during the dry season. *Atmospheric Environment*, *33*, 3919–3930. https://doi.org/10.1016/s1352-2310(99)00134-x

Oleson, K. W., Bonan, G. B., Feddema, J., Vertenstein, M., & Grimmond, C. S. B. (2008). An urban parameterization for a global climate model. Part I: Formulation and evaluation for two cities. *Journal of Applied Meteorology and Climatology*, *47*, 1038–1060. https://doi.org/10.1175/2007jamc1597.1

Oleson, K. W., Bonan, G. B., Feddema, J., & Vertenstein, M. (2008). An urban parameterization for a global climate model. Part II: Sensitivity to input parameters and the simulated urban heat island in offline Simulations. *Journal of Applied Meteorology and Climatology*, *47*, 1061–1076. https://doi.org/10.1175/2007jamc1598.1

Oleson, K. W., Lawrence, D. M., Bonan, G. B., Flanner, M. G., Kluzek, E., Lawrence, P. J., Levis, S., Swenson, S. C., Thornton, P. E., Dai, A., Decker, M., Dickinson, R., Feddema, J., Heald, C. L., Hoffman, F., Lamarque, J.-F., Mahowald, N., Niu, G.-Y., Qian, T., Randerson, J., Running, S., Sakaguchi, K., Slater, A., Stöckli, R., Wang, A., Yang, Z.-L., Zeng, X., & Zeng, X. (2010). Technical description of version 4.0 of the Community Land Model (CLM), NCAR Technical Note NCAR/TN-478+STR, 257 pp.

Oleson, K. W., Bonan, G. B., Feddema, J. J., Vertenstein, M., & Kluzek, E. (2010). Technical description of an urban parameterization for the Community Land Model (CLMU), NCAR Technical Note NCAR/TN-480+STR, 169 pp.

Oleson, K. (2012). Contrasts between Urban and Rural Climate in CCSM4 CMIP5 Climate Change Scenarios. *Journal of Climate*, *25*, 1390–1412. https://doi.org/10.1175/Jcli-D-11-00098.1

Oleson, K. W., Monaghan, A., Wilhelmi, O., Barlage, M., Brunsell, N., Feddema, J., et al. (2015). Interactions between urbanization, heat stress, and climate change. *Climatic Change*, *129*, 525–541. https://doi.org/10.1007/s10584-013-0936-8

Pigeon, G., Legain, D., Durand, P., & Masson, V. (2007). Anthropogenic heat release in an old European agglomeration (Toulouse, France). *International Journal of Climatology*, *27*, 1969–1981. https://doi.org/10.1002/joc.1530

Pigeon, G., Moscicki, M. A., Voogt, J. A., & Masson, V. (2008). Simulation of fall and winter surface energy balance over a dense urban area using the TEB scheme. *Meteorology and Atmospheric Physics*, *102*, 159–171. https://doi.org/10.1007/s00703-008-0320-9

Pigeon, G., Zibouche, K., Bueno, B., Le Bras, J., & Masson, V. (2014). Improving the capabilities of the Town Energy Balance model with up-to-date building energy simulation algorithms: an application to a set of representative buildings in Paris. *Energy and Buildings*, *76*, 1–14. https://doi.org/10.1016/j.enbuild.2013.10.038

Robine, J.-M., Cheung, S. L. K., Roy, S. L., van Oyen, H., Griffiths, C., Michel, J.-P., & Herrmann, F. R. (2008). Death toll exceeded 70,000 in Europe during the summer of 2003. *Comptes Rendus Biologies*, *331*, 171–178. https://doi.org/10.1016/j.crvi.2007.12.001

Sailor, D. J. (2011). A review of methods for estimating anthropogenic heat and moisture emissions in the urban environment. *International Journal of Climatology*, *31*, 189–199. https://doi.org/10.1002/joc.2106

Salamanca, F., Krpo, A., Martilli, A., & Clappier, A. (2010). A new building energy model coupled with an urban canopy parameterization for urban climate simulations-part I. formulation, verification, and sensitivity analysis of the model. *Theoretical and Applied Climatology*, *99*, 331–344. https://doi.org/10.1007/s00704-009-0142-9

Schneider, A., Friedl, M. A., & Potere, D. (2009). A new map of global urban extent from MODIS satellite data. *Environmental Research Letters*, *4*. https://doi.org/10.1088/1748-9326/4/4/044003

Sivak, M. (2013). Air conditioning versus heating: climate control is more energy demanding in Minneapolis than in Miami. *Environmental Research Letters*, *8*. https://doi.org/10.1088/1748-9326/8/1/014050

Stewart, I. D., & Oke, T. R. (2012). 'Local climate zones' for urban temperature studies. *Bulletin of the American Meteorological Society*, *93*, 1879–1900.

Stewart, I. D., Oke, T. R., & Krayenhoff, E. S. (2014). Evaluation of the 'local climate zone' scheme using temperature observations and model simulations. *International Journal of Climatology*, *34*, 1062–1080. https://doi.org/10.1002/joc.3746

Tonoli, G. H. D., dos Santos, S. F., Rabi, J. A., dos Santos, W. N., & Savastano junior, H. (2011). Thermal performance of sisal fiber-cement roofing tiles for rural constructions. *Scientia Agricola*, *68*(1), 1–7. https://doi.org/10.1590/S0103-90162011000100001

Voogt, J. A., & Grimmond, C. S. B. (2000). Modeling surface sensible heat flux using surface radiative temperatures in a simple urban area. *Journal of Applied Meteorology*, *39*, 1679–1699. https://doi.org/10.1175/1520-0450-39.10.1679